LUND UNIVERSITY

—COMSYS—

Battery Energy Storage System Size Optimization for Energy Shifting and Constant Power Delivery - the Benefits of the System Integration with Solar Farms in Sweden

Master's Thesis

By

Andrea Báťková and Noah Situli

Division of Industrial Electrical Engineering and Automation

Faculty of Engineering, LTH, Lund University

Lund, Sweden

ISRN LUTMDN/TMHP-24/5593-SE
ISSN 0282-1990

Abstract

This master's thesis, in collaboration with Comsys AB, examines the optimal size of a Battery Energy Storage System (BESS) for two services - energy shifting and constant power delivery across the four price areas SE1, SE2, SE3, and SE4 in Sweden. For energy shifting applications, the optimal storage capacities were found to be 20 MWh (2 MWh/MW) in SE1, SE2, and SE4. However, a 0.5 MWh/MW storage to power ratio in SE3 was optimal. The energy shifting scenario has a possible market size of 116 40-foot containers, amounting to a market size of $58 million. Under high solar energy penetration scenarios, profitability improved in northern regions. An optimal capacity of 40 MWh (4 MWh/MW) was found for constant power supply, necessitating 397 containers and translating to a market size of $244 million. The study concludes that a 2 MWh/MW ratio for energy shifting and 4 MWh/MW for constant power supply are optimal, suggesting increased solar energy penetration could enhance BESS's financial viability in northern Sweden.

Keywords: Battery Energy Storage System (BESS), Solar Farm, Energy Shifting, Constant Power Supply, Renewable Energy, Sweden, Energy Demand, Power Quality, Profitability, MATLAB, Size Optimization

Acknowledgements

This master's thesis was conducted in collaboration with Comsys AB, and the Division of Industrial Electrical Engineering and Automation, Faculty of Engineering (LTH) at Lund University. The report was written during the spring semester of 2024 within the international master's program in Sustainable Energy Engineering.

We are grateful to Dan Liljengren from Comsys AB for finding a suitable research topic and giving us the opportunity to explore our interests within their company. We extend our heartfelt gratitude to our supervisor, Max Collins, for his invaluable guidance and support at every stage of the project and for his instrumental role in the development of our model.

Furthermore, we would like to thank Mats Alaküla at the Division of Industrial Electrical Engineering and Automation, Faculty of Engineering (LTH) at Lund University, for examining the thesis.

Andrea Báťková

Noah Situli

Lund, June 2024

Table of Contents

List of Figures

List of Tables

List of Abbreviations

Ahr - Ampere-hour
AED - Annual Energy Deficit
BESS - Battery Energy Storage System
CAPEX - Capital Expenditures
C_bN - nominal battery capacity [MW]
CEA - French Alternative Energies and Atomic Energy Commission
CF - capacity factor
cm - centimeter
CPO_f - equivalent operating factor
DOD - depth of discharge
E_{b2g} - energy from battery to grid [MWh]
E_{bcorr} - energy correlated [MWh]
E_b^{left} - energy left from Ebmax [MWh]
E_b^{max} - maximum solar energy that can be stored in battery [MWh]
ED - Energy Deficit
EIFS - numerical order for regulations
E_{pv2b} - solar energy sent from PV to battery [MWh]
E_{pv2g} - solar energy sent from PV to grid [MWh]
E_{pv}^{left} - energy left from E_{pv}max [MWh]
E_{pv}^{max} - maximum solar energy that can be stored in battery [MWh]
EV - Electric vehicle
EUR - euro, €
FLP - Fuzzy Linear Programming
GA - Genetic Algorithm
GAMS - General Algebraic Modelling Systems
HEV - hybrid electric vehicle
i,j,d - loop counters
IEA - International Energy Agency
kg - kilogram
kWh - kilowatt-hour
L - liter
L_{cal} - calendar aging
LCO - Lithium cobalt oxide
LCOE - Levelized Cost of Energy
L_{cycl} - cycle aging
LFP - Lithium iron phosphate
$Li_4Ti_5O_{12}$ (LTO) - Lithium titanite oxide
LIB - Lithium-ion battery
LMO - Lithium manganese oxide
m - meter
m^2 - square meter
MW - Mega-Watt
NCA - Lithium nickel cobalt aluminum oxide
NiCd - Nickel-cadmium
NiMh - Nickel-metal hydride
NMC - Lithium nickel manganese cobalt oxide
NPV - Net Present Value
NREL - National Renewable Energy Laboratory
OPEX - Operational Expenditure
p.u. - per unit
P_b - battery power [MW]
P_cN - battery converter nominal power rating [MW]
P_g - system power [MW]
P_gN - nominal power of the system [MW]
PM - Post Meridiem, afternoon
P_{pv} - PV power [MW]
$P_{pv}N$ - nominal power of solar farm [MW]
PSO - Particle Swarm Optimization Algorithm
PV - photovoltaic
PVGIS-SARAH2 - Photovoltaic Geographical Information System
RBO - Rule-Based Optimization
RES - Renewable Energy Sources
RoR - Rate of Return
S2P - Storage to Power ratio
SEI - Solid Electrolyte Interface
SOC - State of Charge
SOC_{max} - State of Charge maximum
SOC_{min} - State of Charge minimum
SP - Surplus Energy
SPIDER - Simulation Platform for the Integration of Distributed Energy resources
t - time
T_{cell} - cell temperature
Ts - time step
UTC - Coordinated Universal Time
V_d - Decision vector
VRES - Variable Renewable Sources
Wh - Watt-hour
η_b - BESS efficiency

1 Introduction

In this introductory chapter, the general purpose of the thesis is presented. Some background on Battery Energy Storage System (BESS) in power systems and some basics regarding the critical role that BESS will play in the energy mix in smart grids, which is needed to understand the following chapters of the thesis, are given.

1.1 Background

Global energy systems are undergoing a significant transition towards a new paradigm typified by the decentralisation of energy resources, electrification of the transportation sector, and decarbonisation (gradual reduction of carbon intensity) of energy generation parks. The electrical system must ensure not only the availability of energy or electrical supply but also its quality, and all of this must be done at the lowest feasible cost (Tejero-Gómez and Bayod-Rújulaz, 2023). Electricity is a primary need of human society. All activities are dependent on the availability of power. According to IRENA, by 2050, electricity is projected to become the primary energy source, accounting for nearly 50% of total consumption. This would result in a more than doubling of gross electricity consumption (IRENA, 2019) In recent years, energy production from renewables has also increased due to falling costs of technologies such as wind and photovoltaic (PV) solar power. The current grid consists of different types of loads as well as generation sources. Due to the high penetration of renewable energy, conventional electric generators have been replaced mainly by renewable energy generators in power generation. Unfortunately, the lack of constant power resulting from the intermittent and stochastic nature of renewable resources makes it challenging to secure a reliable power system with a high penetration rate of renewable energy generators (Yoo, Jang and Jung, 2022).

In 2022, 23% of the energy consumed in the EU came from renewable sources. A robust increase in solar power was a significant factor in this increase, which came from a level of 21.9% in 2021 (EEA, 2024). The share is further boosted by a decrease in non-renewable energy consumption in 2022 due to high energy prices; nevertheless, growth in renewable energy is predicted in Europe. A comprehensive overhaul of the European energy system is necessary in order to meet the new target of 42.5% by 2030, which calls for more than double the rates of renewable energy deployment observed during the previous ten years (EEA, 2024). However, as the amount of energy generated from renewable sources increases, power systems must contend with issues with stability and flexibility (the capacity of power systems to tolerate disruptions over a short time). In this context, a smart grid is an electric power system that effectively delivers secure, affordable, and sustainable electricity supplies by integrating the behaviour and actions of network users and other stakeholders. In addition to using distributed computing, sensors, actuators, and information exchange and control technologies, the grid also requires that all network users—consumers, generators, and storage owners—be able to act in a way that is beneficial to the network. As a result, it is

crucial that renewable energy generation contributes to the stability and dependability of the system, and interconnection standards may increasingly demand this (Tejero-Gómez and Bayod-Rújulaz, 2023).

One factor affected is the power system flexibility. The International Energy Agency defines power system flexibility as the response speed and anti-interference ability of the power system in the face of predicted fluctuations and disturbances outside the forecast (Yao *et al.*, 2022). In this context, anti-interference means the ability of the power system to maintain a stable and reliable operation in the face of unexpected disturbances or fluctuations that were not anticipated in the forecast. This capacity has traditionally been supplied by conventional thermal power plants and hydropower, but as their shares in the power system decrease, other sources must provide power system flexibility. One technological solution that can provide flexibility is energy storage due to its potential to charge and discharge electrical energy. One potential flexibility provider is BESS. As the costs of these systems have been declining, their role is likely to increase even further in future power systems (IEA, 2020).

Contrary to popular belief, a generation plant's ability to provide minimally secure or predictable power during periods of peak demand is what determines how much it contributes to supply security, not its installed power. Minimally secure means the lower threshold or baseline level of power that can be guaranteed with a high degree of confidence. The "safe" power is referred to as firm power. Firmness is defined as the greatest force that a high degree of probability can overcome (Tejero-Gómez and Bayod-Rújula, 2023). Firm power depends on several variables, including the availability of the primary energy sources (fuel, wind, water, etc.) and the maintenance performed on the installation or its operating system (frequency of stops and starts, etc.). Thus far, firmness has been associated with controllable technologies like gas or nuclear power, which are independent of outside forces and have firmness coefficients greater than 95% (Garside, 2022). This is not the case for renewable energy sources without storage, such as wind and solar power, since their ability to generate electricity is entirely dependent on resource availability. As a result, it is impossible to predict how much electricity these sources will be able to contribute to the system over the medium term. Wind energy's firmness cycle is typically estimated to be 9%, while photovoltaic solar energy (without storage) has a value of 0% (Tejero-Gómez and Bayod-Rújula, 2023). The traditional method of solving the variability issue in renewable energy installations involves incorporating more adaptable resources, like big generators and Volt-Amps Reactive (VAR) control devices. VAR Control helps address variability and intermittence in renewable energy installations by managing reactive power in the electrical grid. This is essential for maintaining voltage stability and overall power quality (Tejero-Gómez and Bayod-Rújula, 2023).

There is also the risk that in a situation where there is a high penetration of renewable technologies into the system, particularly when solar energy is used, simultaneous generation of renewable energy could lead to overgeneration at midday and curtailments or the loss of electricity that would otherwise be wasted due to low demand. Photovoltaic installations can be given stability through the integration of storage systems with PV plants, allowing for

increased integration into electrical networks. In other words, power generation in hybrid PV systems with storage is more dispatchable, dispatchable, and predictable—that is, more grid-friendly (Bayod-Rújula, Haro-Larrodé and Martínez-Gracia, 2013). When battery energy storage systems (BESS) are integrated into photovoltaic plants, the renewable resource becomes more reliable and may have a longer duration of continuous power supply. According to a forecast, solar power and storage combined could reach 30 TWh globally by 2050, far exceeding any other storage capacity (Tejero-Gómez and Bayod-Rújula, 2023). This suggests a transformative shift in the energy sector towards renewable sources in the future hence the importance of exploring BESS applications.

1.1 Purpose and goal of the study

While there are several ways for a solar farm with BESS to generate income, two popular strategies are trading energy and trading power. Energy trading entails buying and storing energy when the spot prices are low and selling the energy when the spot prices are high. On the other hand, trading power means buying and selling power for the purposes of the frequency market. An additional source of revenue for producers is the provision of ancillary services, i.e. compensating reactive power, symmetrizing asymmetric loads, and compensating unwanted frequency components. Ancillary services balance supply and demand on electricity networks, prevent grid overload and ensure frequency, balance, stability, and security (Dustmann and Bito, 2009).

This thesis provides a preliminary screening for COMSYS AB, to evaluate the financial viability of various BESS options and identify potential risks and advantages associated with each option. Although optimising BESS sizes for solar parks in Sweden is the primary focus of this study, profitability considerations will also be investigated.

The main aim is to identify the optimal BESS size for two key services: energy shifting and constant power supply in relation to solar farm capacity. Additionally, this project will focus on evaluating the financial viability and BESS market size. The main research questions are:

1. What is the optimum size of the BESS with respect to solar farm capacity for energy shifting and constant power applications?
2. What is the estimation of the market size and profitability (based on ROR) of BESS integration with solar parks in four price areas of Sweden?

1.2 Delimitations

The master thesis project is limited to locations in Sweden, 4 locations with associated solar irradiation and spot prices are used in simulating the performance of a grid-connected PV plant in 4 price areas of Sweden (SE1, SE2, SE3, and SE4). However, it is important to note that the methods and approach can be used for any location provided solar irradiation and spot prices are known. The economic analysis includes the main aspects of the project. The ROR is used as the main financial parameter to determine the profitability of BESS

installation in existing solar parks in Sweden. Since receiving accurate data on components is often difficult, the material cost is instead included as statistical costs per installed kW_p found in NREL. The thesis work only considers the optimization of BESS installations and determining the market size in energy shifting and constant power applications. Furthermore, other storage installations, such as flywheel, pumped storage, etc are not in the scope of this work.

1.3 Outline

This thesis is organized as follows: Chapter 2 provides an overview of the literature review related to the topic under analysis. This chapter review different battery technologies and their degradation over time during their lifespan. It explains the factors that contribute to battery degradation. Furthermore, it explains different BESS optimization techniques and their significance to the study in detail. Chapter 3 includes the materials and methods used to create the thesis. Foundation research papers upon which the work is built are described, followed by the description of the MATLAB model developed by the authors of this thesis. Chapter 4 presents the paper's analysis and discussion of the site-specific PV plants in Sweden using BESS for energy shifting and constant power application. The thesis' conclusions are finally explained in Chapter 5, which also summarises all of the research's findings, the thesis's limitations, and suggestions for more study.

2 Literature Review

This chapter aims to review different battery technologies and their degradation over time during their lifespan. It explains the factors that contribute to battery degradation. Furthermore, it explains different BESS optimization techniques and their significance to the study in detail.

The worldwide movement to reduce greenhouse gas emissions has incentivized the deployment of renewable energy power plants. China's 14th Five-Year Plan for Renewable Energy includes a plan to reach the goal of 33% of electricity being generated by renewable energy sources (RES) by 2025. The United States introduced tax credits to support renewable energy development in 2022. The targets of the European Union were updated in the RePowerEU plan as a response to Russia's invasion of Ukraine and resulting concerns for energy security. The new plan strives to reach 45% of renewables by 2030, while many individual countries have also reviewed their energy targets. India has announced the goal to reach 50% renewable electricity share by 2030 and net zero emissions by 2070. According to IEA, by 2028, the global power mix will be made out of 42% renewable energy sources, 25% of this share being solar PV and wind power (*Renewables - Energy System*).

From the power grid perspective, the rapid development of solar and wind energy projects poses a challenge due to their intermittent nature. Shifting towards variable renewable sources (VRES), i.e. wind and solar, means shifting from centralized power generation plants powered by a readily available high-energy source to a distributed power generation of an intermittent nature. The fossil-fuel power plants are large-scale electricity sources, whose location was planned based on demand, and they actively participate in control of voltage and frequency. On the other hand, the VRES location is highly reliant on geographical and meteorological conditions (e.g. offshore wind farms). This shift can have a negative effect on power quality, including flicker, voltage fluctuations, frequency disruptions, harmonics, and power factor reduction, and in extreme cases, even lead to a complete blackout (Braga, 2023) (Datta, Kalam and Shi, 2021). Several countries have implemented mandatory grid codes to ensure power quality, including limits for fault-ride-through, ramp rate, frequency and voltage control capability, etc. (Datta, Kalam and Shi, 2021).

In Sweden, the connected facilities need to comply with the Commission Regulation (EU) 2016/631 of 14 April 2016, establishing a network code on requirements for grid connection of generators. This regulation applies to new power-generating modules which are considered significant. The significance determination points are presented in the document, where 4 categories are defined based on their voltage and power rating. The storage devices, except for pump-storage power generation, are not regulated in this document. The connected facilities also need to comply with the Swedish Electricity Act, and the Swedish secondary regulation EIFS 2018:2. The storage devices are not regulated in the EIFS 2018:2 either. (*Information regarding network codes for grid connection*, 2020) (*Commission Regulation (EU) 2016/631 of 14 April 2016 establishing a network code on requirements for grid connection of generators (Text with EEA relevance)*, 2016). The Act amending the Electricity

Act (1997:857) states that a grid operator (nowadays Svenska Kraftnät) may not own, develop, manage, or operate an energy storage facility unless being granted an exemption by the government (*Lag om ändring i ellagen (1997:857) | Svensk författningssamling*, 31.05.2022).

A battery energy storage system (BESS) is considered to be one of the most optimal solutions to ensure power system stability in high VRES penetration regions (Datta, Kalam and Shi, 2021). The BESS can regulate the output of VRES and providing numerous services, including:

- *energy arbitrage* - buying electricity during off-peak hours to sell it during peak hours for increased profitability, alternatively storing energy that would otherwise be curtailed,
- *electric supply capacity* - utilizing BESS to reduce the need to install new central station generation capacity, avoiding the accompanied investment of the new capacity,
- *regulation/load leveling* - regulating the power output of the system to match the demand to help maintain the system frequency,
- *backup reserve* - the stored energy could be accessed by the grid operator in case of unexpected unavailability of a generation unit,
- *voltage regulation* - BESS can help maintain a stable voltage source in the grid by discharging/charging the battery as a response to voltage swells/sags. The voltage surges occur during high PV generation and low load which results in reverse power flow in the network, but a single-point connection of large-scale distributed generation may also result in voltage violations. There are some other technologies which can help prevent these voltage violations, for example PV converter reactive power generation, voltage regulator, or transformer tap adjustment (Datta, Kalam and Shi, 2021).
- *black start* - energy is used as an active reserve to help energize the transmission and distribution lines and bring power generation units back on line,
- *transmission upgrade deferral* - investments into transmission system upgrades can be delayed/reduced by strategically placing energy storage units to prevent overloading a transmission node,
- *transmission congestion relief* - system congestion happens when the energy from the generation units cannot be delivered to loads due to transmission system limitations, energy storage can be used to avoid the resulting charges and costs,
- power quality - energy storage protects consumers downstream from short-term events affecting power quality, including voltage and frequency fluctuations, harmonics, or low power factor (Asian Development Bank, 2018).

Increasing solar energy penetration, characterized by zero marginal cost may eventually result in the so-called “cannibalization effect”. This is tied to the merit-order effect which dictates the wholesale electricity price (the cost of energy from distributor to retailer (‘Wholesale Price - Definition, Wholesale vs. Retail Price’, 2023)). Compared to other non-VRE technologies, solar parks (and wind technologies) have almost no operating and

maintenance costs, thus lower prices (López Prol, Steininger and Zilberman, 2020). The merit order prioritizes the energy sources with the lowest cost and supplements the rest of the demand from other sources (such as nuclear). In such an instance, the resulting wholesale price would be the unit price for nuclear energy or any other higher price depending on the employed technology. However, if solar energy can satisfy the whole demand, it is the sole technology to dictate the wholesale price, meaning there would be no other source to keep the prices higher (and make it more profitable for solar energy investors). This essentially means that the higher the solar energy penetration, the lower the income from the installations (*Setting the power price: the merit order effect*, 2015). With the investment costs for solar panels still relatively high, this can significantly hinder the deployment and overall profitability of the system. To mitigate this effect the work by Prol et al. (2020) suggests that for the case of solar, the best solution appears to be low-cost storage. Moreover, the cannibalization effect indicates that in the future the service of peak shaving and supplying solar energy at a constant level might be crucial in the transition to low-carbon emission technologies and ensuring their economic profitability (López Prol, Steininger and Zilberman, 2020).

2.1 Battery technologies

In recent years, the Battery Energy Storage System (BESS) has become more popular due to its ability to provide energy simply, safely, and reliably when it is needed. There are different battery technologies with different workings and characteristics.

The basic working principle of batteries is creating a chemical reaction between two electrodes, a cathode and an anode, which has the potential to store energy. During the process of charging, electrical energy is converted into chemical energy and stored within a battery. This process is then reversed when there is a need for electricity, and known as discharging. Different types of batteries are suitable for different applications due to their power, energy, response time, and efficiency characteristics (Ingman and Sivers, 2023). The most common battery technologies are lead acid, sodium sulfur, flow batteries and lithium-ion batteries.

2.1.1 Battery characteristics

The following battery specifications or characteristics are crucial to battery system sizing, design and operation. The following definitions of battery parameters as defined by (Mehar, Singh and Gupta, 2023), are critical in understanding battery operation.

Capacity: Defined as the maximum amount of energy that a battery can hold in a certain period of time. A battery's capacity to store power is commonly measured in watt-hours (Wh), kilowatt-hours (kWh) (Mehar, Singh and Gupta, 2023).

Energy density: A key focus of battery research is achieving the best energy density possible, which indicates that a battery can hold more energy while maintaining its same

weight and dimensions. Energy density is determined by the quantity of energy a device can store per unit of volume (Wh/L). Some authors refer to this feature as specific energy, which is expressed as Wh/L or Wh/kg (Mehar, Singh and Gupta, 2023).

Power density or Specific power: It's the ability to deliver a high power and indicates loading capability. Batteries for power tools are made for high specific power and come with a reduced specific energy (Mehar, Singh and Gupta, 2023).

Performance: Performance is a critical parameter of batteries, it reflects how efficiently and effectively a battery can store and deliver energy. Battery performance is characterized by power density and energy density, both of which are influenced by temperature, cycling, and age. Extreme temperatures (both high and low) negatively affect performance by altering chemical reaction rates and increasing internal resistance. Repeated charging and discharging cycles degrade the electrodes and electrolyte, reducing power and energy densities over time. Natural aging processes, exacerbated by poor storage conditions, also leads to performance decline even without active use (Nykvist & Nilsson, 2015).

State of Charge (SOC): The State of Charge refers to the current level of charge in the battery relation its total capacity. SOC is normally expressed as a percentage and calculated as a ratio of remaining energy in the battery at a given time to maximum possible energy (Amon, 2020).

$$SoC(t) = \frac{Q_{remaining}(t)}{Q_{max}(t)} x100\ [\%]$$

State of Health (SOH) : State of Health is estimation of the battery's maximum level of charge compared to its initial value when it was first used. SOH is also expressed as a percentage and calculated as a ratio of maximum energy storing capacity to nominal capacity (Amon, 2020).

$$SoH(t) = \frac{Q_{max}(t)}{Q_{nominal}(t)} x100\ [\%]$$

Depth of Discharge (DOD): It is defined as the amount of charge discharged or removed from the battery at a given state in relation to the total charge that a battery can store. DOD is expressed as a percentage and is calculated as below (Waag & Sauer, 2009).

$$DOD(t) = \frac{\mathrm{Q}(t)}{Q_{max}(t)} x100\ [\%]$$

C-rate: The C-rate is the ratio of the charging or discharging electrical current in Amperes (Bašić, Bobanac & Pandžić, 2023)**.**

Lifespan: Another aspect to consider is the durability of the battery, which is determined based on how many charging repetitions it can withstand. The aim is to attain batteries that can withstand longer during the loading and unloading period. This reflects cycle life and longevity and is related to factors such as temperature, depth of discharge, and load (Mehar, Singh and Gupta, 2023).

Safety: This relates to factors such as the thermal stability of the materials used in the batteries. The materials should be able to sustain high temperatures before becoming unstable. Instability can lead to thermal runaway, in which flaming gases are vetted. Fully charging the battery and keeping it beyond the designated age reduces safety (Mehar, Singh, and Gupta, 2023).

Cost: Cost is a huge factor when selecting the type of lithium-ion battery (IRENA, 2017).

2.2 Types of Batteries

2.2.1 Lead acid batteries

Lead acid batteries are the most widely deployed rechargeable batteries in terms of technology, based on the number of installations and cumulated installed capacity. Lead acid batteries are known to have a good cost-performance ratio in a wide range of applications. However, they have a relatively low energy density, are heavy, typically do not respond well to deep discharging, and lead may be a restricted material in some applications or locations due to its toxicity (Mehar, Singh, and Gupta, 2023).

There are two main design forms of lead acid batteries available “flooded” (often also called “vented”) and valve regulated (often also referred to as “sealed”). At present, lead acid batteries are used in multiple applications, including as starter batteries in cars, in uninterrupted power supply systems, as traction batteries in forklifts or golf carts and in off-grid applications such as communication towers in rural areas. These batteries have been widely applied to the deployment of renewables, notably in solar home systems in off-grid applications around the world (Feder, Hlavac and Koster, 1993).

2.2.2 Nickel-Cadmium batteries (Ni-Cd)

Nickel-cadmium batteries are considered outdated and are currently being substituted by nickel-metal hydride batteries (NiMH). Despite these batteries containing more energy density, they have many drawbacks like lower life span, durability, great memory influence and using cadmium which is highly expensive (Mehar, Singh and Gupta, 2023).

2.2.3 Nickel-Meatal Hydride batteries (Ni-MH)

Nickel-metal hydride batteries (Ni-MH) have great room for advancement compared to Nickel-cadmium batteries. Ni-MH batteries seem to be the preferred option for use in hybrid electric vehicles (HEV), electric vehicles (EV) and fuel cell EVs. In addition, the Toyota RAV4 EV also came in a nickel-metal model (Mehar, Singh and Gupta, 2023).

2.2.4 Lithium-ion battery technology

Lithium-ion batteries (LIBs) come in various forms, but they all have a positive electrode (cathode) composed of various materials and lithium metal oxide. Lithium iron phosphate ($LiFePO_4$) and lithium titanate oxide ($Li_4Ti_5O_{12}$) are two common cathode materials. Due to their respective qualities, the two chemistries are ideal for grid applications. Typically, carbon serves as the negative electrode, or anode, for most LIB chemistries. A polymeric substance that separates the cathode and anode allows ions to move between the two electrodes during charge or discharge. Lithium salt-based electrolyte is also submerged in the electrodes (Ingman and Sivers, 2023).

Characteristics such as specific power, specific energy, lifetime, cost, and performance vary among LIB chemistries. Figure 1 and Table 1 compare these characteristics among six LIB chemistries - lithium cobalt oxide (LCO), lithium manganese oxide (LMO), lithium nickel manganese cobalt oxide (NMC), lithium iron phosphate (LFP), lithium nickel cobalt aluminum oxide (NCA), and lithium titanate oxide (LTO). Unlike lead acid batteries, that has an enduring legacy in the automotive sector, lithium-ion batteries have increasingly been used in portable electronics, electric vehicles and grid storage applications (Rakhimov *et al.*, 2024).

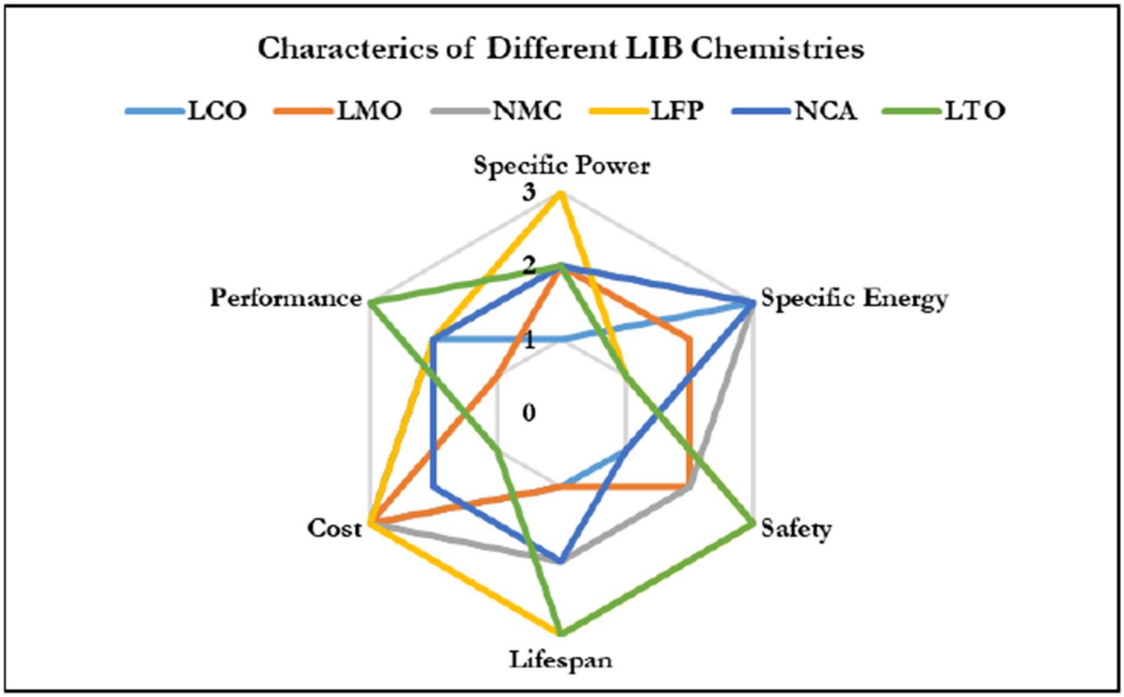

Figure 1 Comparison of six LIB chemistries (Ingman and Sivers, 2023)

Table 1 Pros and Cons of six LIB chemistries (Ingman and Sivers, 2023)

Technology	**Energy density (Wh/Kg)**	**Cycle life**	**Description**
LCO	200	500-1000	LCO has high specific energy and low cost, making it the preferred choice for laptops and mobile phones. The low specific energy, low safety and short lifetime makes it less favorable for other use cases.
LMO	100-150	300-700	LMO has moderate specific power and energy and low cost. The disadvantages of LMO is the low performance and short lifetime.
NCA	200-260	500	NCA has one strong advantage of high specific energy. Apart from this, the other parameters are moderate apart from its low level of safety.

LTO	50-80	3000-7000	LTO has long lifetime, high safety, and good performance. LTO has a longer cycle lifetime, reaching as high as 20 000 equivalent cycles. The major disadvantage of LTO is the extremely high price.
NMC	150-220	1000-2000	NMC has high specific energy and moderate lifespan and performance. The disadvantage of NMC is cost.
LFP	90-120	≥2000	LFP has high specific power and lifespan. However, the cost is high and the safety is low

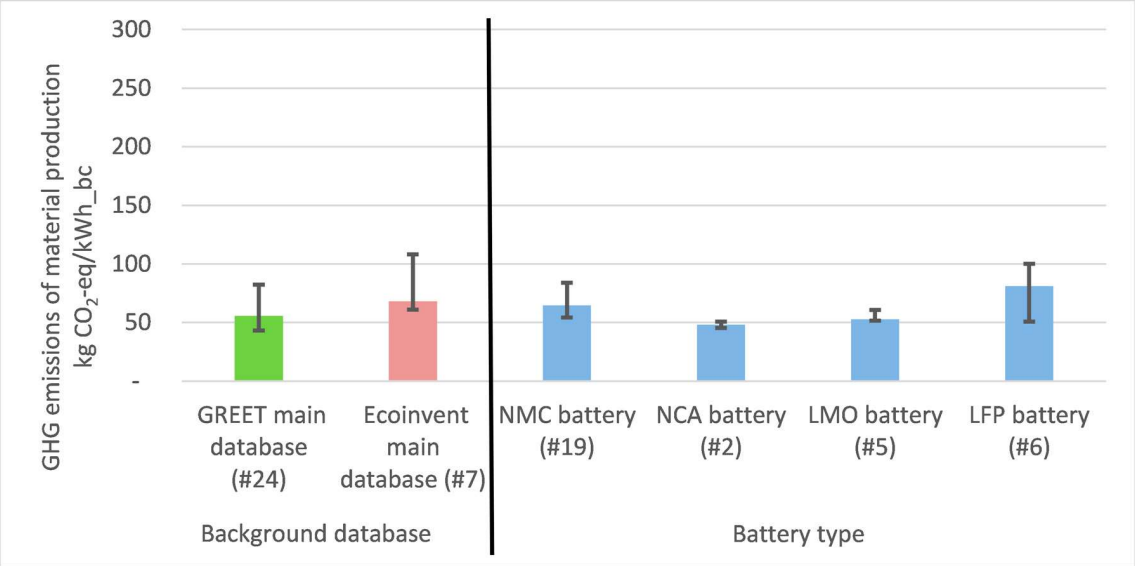

Figure 2 GHG emissions comparison of material production between databases and battery types ((results based on median, 25%-quantile, and 75%-quantile) (Christian Aichberger & Gerfried Jungmeier, 2020)

Two chemistry types mostly used in stationary applications are LFP and NMC. As the figure above clearly shows, LFP is known for its high safety, long lifetime, high specific power, and low cost. The only significant disadvantage over other chemistries is the low specific power. LFP is also known for its superior thermal stability and lower environmental impact than other LIB chemistries. No other chemistry combines low cost and long lifetime, making LFP an excellent choice for stationary applications**.** NMC offers the same low cost as LFP but with a shorter lifetime, lower safety, and lower specific power. The main advantage of NMC over LFP is the specific energy, which is much higher and can be tailored for high power or high energy purposes (Ingman and Sivers, 2023). This thesis will focus on Lithium-ion (LIBs), with a particular emphasis on LiFePO4 (LFP), which is a specific type of LIB chemistry. This battery is widely regarded as the most suitable choice for large-scale

stationary applications due to its calendar lifetime, large number of lifetime cycles, low self-discharge, and high efficiency (Naumann *et al.*, 2018).

Figure 2 shows the results from research conducted by Christian Aichberger & Gerfried Jungmeier (2020) on GHG emissions of material production by different battery types and background databases.

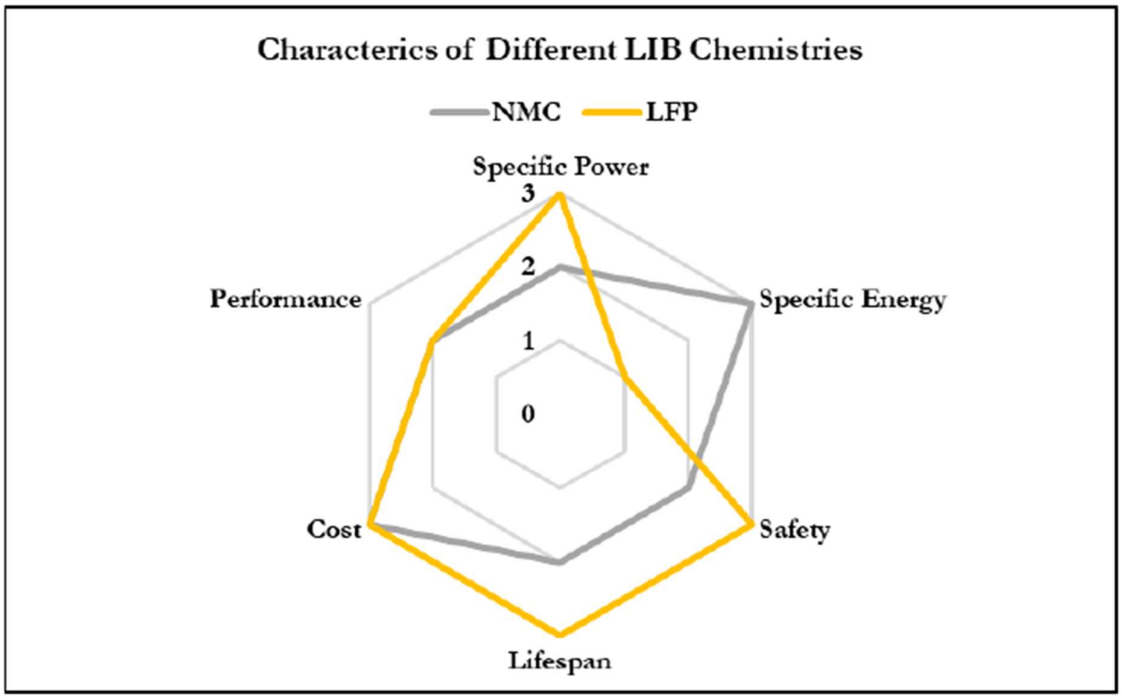

Figure 3 Comparison of NMC and LFP chemistries (Ingman and Sivers, 2023)

2.3 Battery degradation

Degradation and capacity fade in Lithium-ion batteries significantly impact the operational and maintenance costs in various applications. For instance, in the context of electric vehicles, studies have shown that factors such as cyclic aging (Xu *et al.*, 2018), depth of charge and discharge rates (Cao *et al.*, 2020) and the effects of repeated charging and discharging (Shi *et al.*, 2018) all contribute to increased operational expenses. in a similar manner, in applications like energy arbitrage, grid-scale battery storage operation, and microgrid management (Khalilisenobari and Wu, 2021), it is crucial to consider the cost of battery degradation in operational decisions.

Battery degradation models play a crucial role in our understanding of their impact on operational costs. Comprehensive studies on a variety of models have been proposed, including semi-empirical models for Lithium-ion batteries (Xu *et al.*, 2018). This paper combines theoretical analyses and experimental observations and proposes an accurate model for determining battery life assessment. substantial research on cycle-based degradation models (Shi *et al.*, 2018) and incremental degradation estimation methods (Sandelic,

Sangwongwanich and Blaabjerg, 2022) provides us with a comprehensive understanding of how battery aging affects operational expenses and can guide decision-making processes to mitigate degradation-related costs, thereby empowering us with the knowledge to make informed choices. The figure below illustrates the impact of DOD on cycle life. As clearly shown, increasing the DOD reduces the cycle life for a battery.

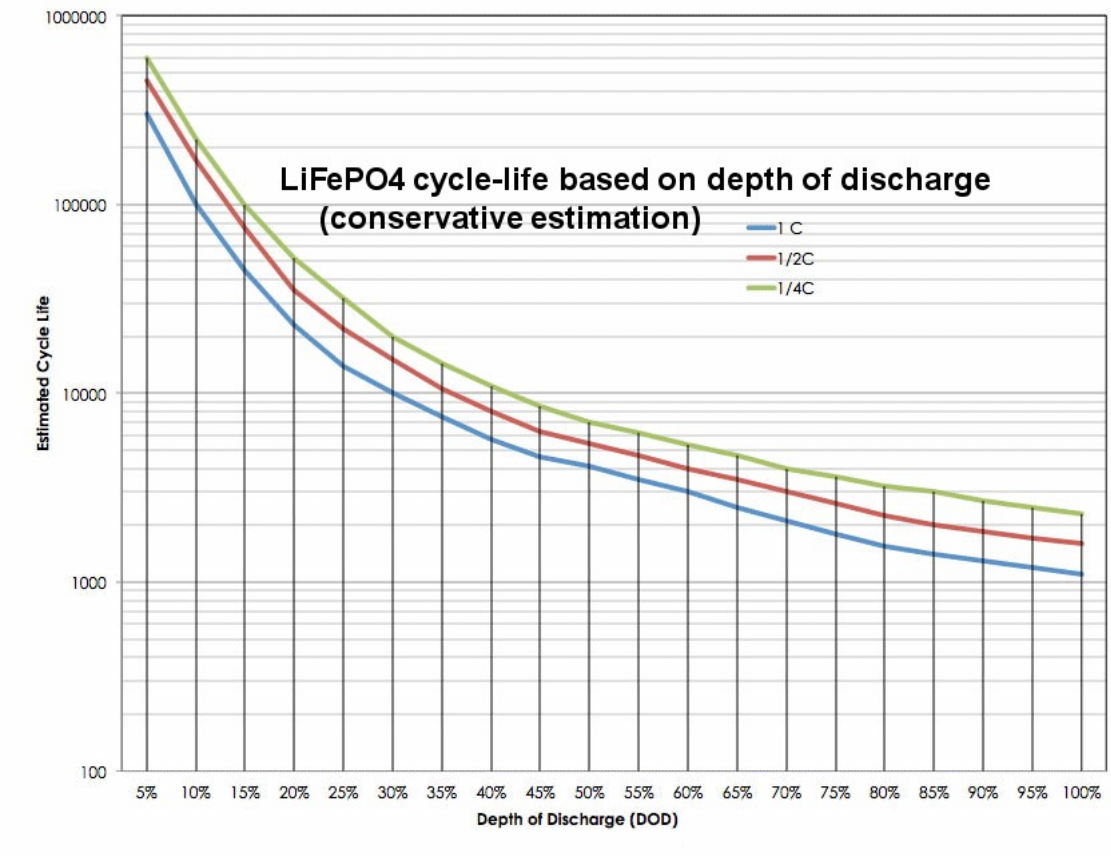

Figure 4 Estimation of the cycle life based on the Depth of Discharge and discharge rate (gwl-power, 2024)

2.3.1 SEI thin formation mechanism

The solid electrolyte interface (SEI) expansion is the primary cause of degradation and capacity fade in lithium-ion batteries. This interface, which forms a protective film between the electrodes and the electrolyte, is crucial for battery operation. The SEI film acts as a barrier, impeding the interaction of lithium ions with the electrodes. However, if the film thickens, it can lead to cell degradation. Despite this, the SEI film is essential as it prevents further undesirable reactions between the electrode and the electrolyte, ensuring the battery's longevity (Ingman and Sivers, 2023). The figure below illustrates the SEI formation in lithium-ion batteries.

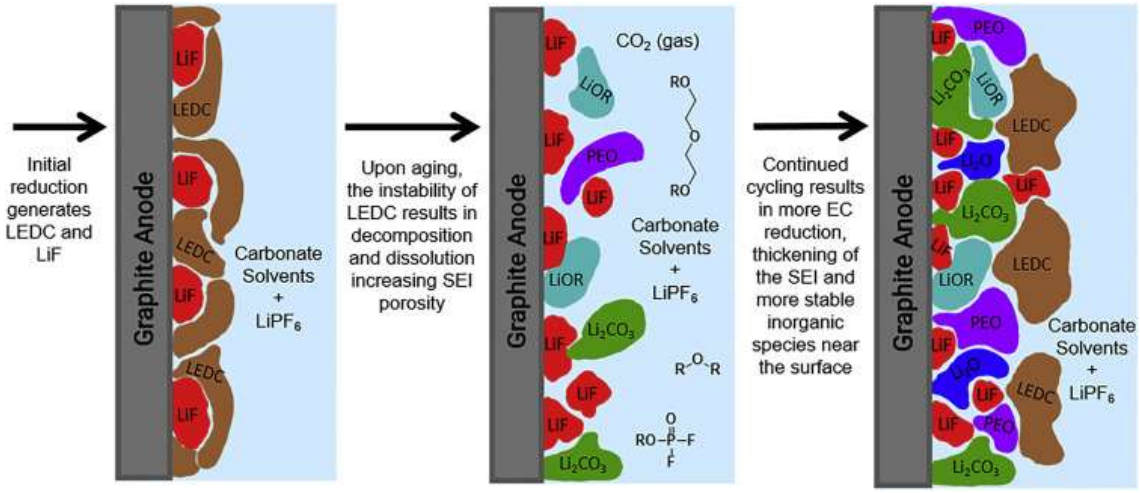

Figure 5 Illustration of SEI model in the lithium-ion battery (Heiskanen, Kim & Lucht, 2019)

The growth of the SEI film is not a static process but rather contingent upon battery usage patterns. Elevated temperatures and states of charge can exacerbate its formation, leading to accelerated cell degradation. While the SEI growth is commonly associated with the carbon electrode in Li-Ion cells, similar occurrences have been noted on the lithium metal oxide side. The chemical reactions underlying SEI formation deplete the available supply of lithium ions, resulting in a loss of active material and reduced cell capacity, a phenomenon that can be influenced by how batteries are used (Ingman and Sivers, 2023).

Apart from the SEI growth mechanism, lithium-ion batteries are also affected by a phenomenon known as Lithium plating, which normally occurs due to overcharging the battery. According to (Xie and Yang, 2023), lithium battery plating is a critical issue affecting the performance and safety of lithium batteries, particularly during fast charging processes. This phenomenon can also lead to capacity reduction. Even though lithium plating is most pronounced in high energy density battery technologies, it is proven to be a challenge to detect it in real-time during battery charging (Koleti, Dinh and Marco, 2020). In the recent past, several techniques have been developed to mitigate the effects of lithium plating in batteries. Techniques include the development of optimal charging protocol and using reference electrodes for plating onset monitoring (Liu, Gao and Liu, 2021).

In this thesis, it is assumed that factors such as overcharging, over-discharging (two phenomena that involve charging or discharging batteries outside the range of the cut-off voltage) or operating the battery at extremely high or low temperatures are not taken into account.

2.3.2 Calendar and Cycle aging

The battery degradation process is considered to be a nonlinear process with respect to time and stress cycles due to its dependence on external stress factors such as time, temperature, charging, discharging, and the current state of life. The process of charging and discharging batteries is likened to the fatigue process of materials subjected to cyclic loading (Xu *et al.*, 2018); each cycle causes independent stress, and the loss of battery life is the result of the

accumulation of all cycles. Total battery aging is made up of calendar aging and cycle aging. Calendar aging is defined as the battery's inherent degradation over time, and the rate at which this occurs is affected by the temperature and the SOC of the battery. Therefore, calendar aging can be expressed as a function of average SOC, time, and cell temperature (Xu *et al.*, 2018).

$$Lcal = f(SOC, t, Tcell)$$

On the other hand, cycle aging is the battery life lost each time the battery cycles between charging and discharging. Cycle aging is affected by the depth of discharge (DOD), the average SOC of the cycle and cell Temperature. The cycle aging is then expressed as follows (Xu *et al.*, 2018)

$$Lcyc = \sum ni.f(DOD, SOC, Tcell)$$

2.3.3 State of Charge

The SOC range, which denotes the charge levels during charging and discharging, plays a crucial role in battery health. Both shallow (high SOC) and deep (low) states can have adverse effects, with shallow states prone to corrosion and oxidation reactions, especially in high-temperature environments (Pi and Liu, 2024).

According to (Xu *et al.*, 2018), a high SOC indicates high degradation levels and a lower rate at low SOC. The figure below shows calendar aging with varying SOC at 25°C. The remaining capacity entails the amount energy that BESS can hold after a certain period of time.

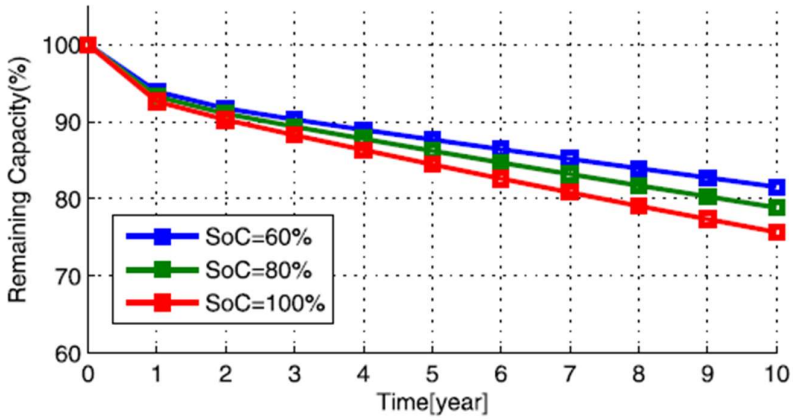

Figure 6 Calendar aging with varying SOC at 25°C (Xu et al., 2018)

2.3.4 Temperature

Temperature variations also play a vital role in battery performance. Temperature gradients in battery packs can lead to unbalanced charge and discharge currents, affecting battery life and efficiency (Raijmakers *et al.*, 2019). Higher operating temperatures tend to reduce battery

capacity more than lower temperatures. Figure 7 shows calendar aging with varying temperatures at 50% below SOC.

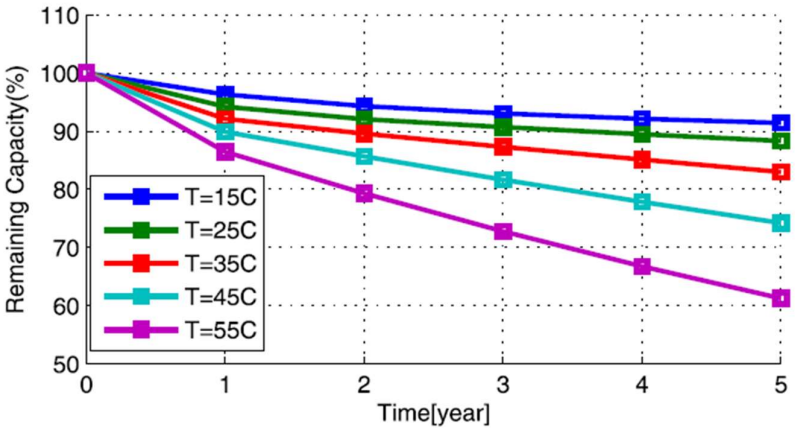

Figure 7 Calendar aging with varying temperature at 50% SOC (Xu et al., 2018)

2.3.5 Charge rate

The common expression for charge rate is the concept of C-rate. C-rate indicates the relationship between charging power and battery capacity. For example, when the power value in kW is equal to the battery pack capacity in kWh, 1C is the charging power (current) for one hour. It would take 30 minutes to fully recharge at 2C (Bašić, Bobanac & Pandžić, 2023). The figure below shows the variation C-rate and SOC for a modern EV.

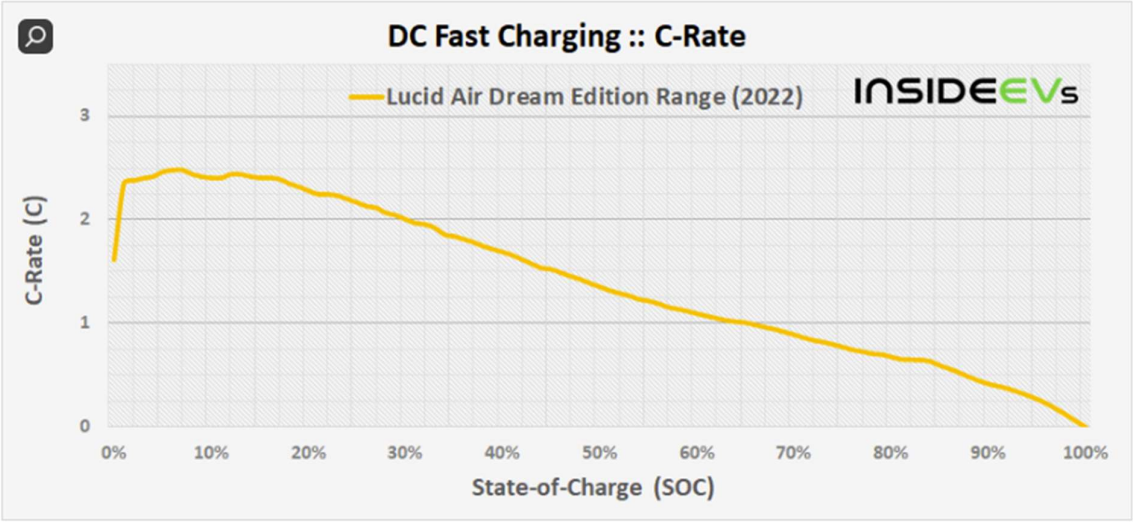

Figure 8 Variation of C-rate and SOC for a modern EV (InsideEVs, 2024)

Even though charge rate is not a factor in the aging model, its influence on battery temperature and longevity is significant. Higher charging rates can result in increased temperature through ohmic heating during charging, thereby affecting the battery's thermal properties and overall performance (Yan *et al.*, 2011). Charging a battery at high rates can

also elevate the battery temperature, potentially leading to thermal runaway and reduced battery life (Sandhya Lavety; Ritesh Kumar Keshri; Madhuri A. Chaudhari, 2020)

2.4 Optimization techniques

Deploying the BESS is accompanied by a significant investment so optimal sizing is crucial for determining the ideal cost-to-income ratio. However, optimal sizing can be challenging due to a dependence on various factors, including control strategy, BESS efficiency and degradation of the battery over its lifetime, intermittent nature of the energy sources, and electricity prices (Richard, Pivert and Bourien, 2020). Various size optimization techniques have been researched over the years and are described below.

2.4.1 Probabilistic approaches

Usually regarded as one of the least complicated sizing methods due to the possibility of optimizing a maximum of two system parameters, which simultaneously constitutes a major drawback. However, this method is highly suitable for applications where only limited data is available (Hannan *et al.*, 2021). The base idea for this method is to use the stochastic nature of renewable resources, such as solar, in order to optimize BESS for selected criteria. A usual approach is to create a generation profile of the power plant (such as a solar PV farm) and combine it with a load profile to make a risk model. Against this risk model, the performance criteria may be optimized (Yang *et al.*, 2018).

2.4.2 Rule-based approaches

In the rule-based optimization method (RBO), the solution is obtained by defining a set of rules. One of the most dominant types of RBO for BESS is the fuzzy logic which is especially significant since the increase of uncertain parameters has no major effect on the size of the problem (Muqbel *et al.*, 2018).

2.4.2.1 Fuzzy logic

The BESS size optimization with power, energy capacities, and long-term profit was studied by (Muqbel *et al.*, 2018) using fuzzy linear programming (FLP). In their work, charging and discharging constraints are considered and the model is compared with the model obtained by a deterministic approach. It should be noted that in the case of the deterministic approach, the vector of uncertain parameters is neglected, and historical data are used instead to estimate the parameters. The results of the case study show that the deterministic approach shows higher optimal power capacity and expected profit, but lower optimal energy capacity than the fuzzy counterpart. According to the authors, the expected profits of the fuzzy model being less than that of the deterministic model indicates that when the price forecast is precise, the deterministic model obtains better results, which is to be expected. However, a study for realized profits was also undertaken in the study showing different results. In this part, the fuzzy model shows higher realized profits than the deterministic model. Moreover, for the fuzzy model, the expected and realized profits were much closer than for the

deterministic model. These results suggest that the fuzzy approach is more suitable for the prediction of actual profits compared to the deterministic method (Muqbel *et al.*, 2018).

2.4.3 Deterministic approaches

Also referred to as analytical methods is one of the most widely used techniques for BESS size optimization. The key concept of these methods is to analyze a series of power system configurations with the system elements varied being those that are being optimized against the set performance criteria. These methods are usually implemented by repetitive simulations performed over a set amount of time for the relevant components, often requiring large computational resources when solving for smaller time intervals (Yang *et al.*, 2018). The flowchart describing the base process of deterministic approaches is shown below.

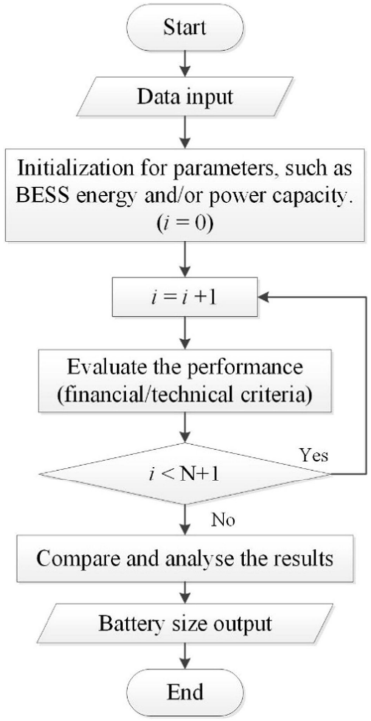

Figure 9 Deterministic method process description (Yang et al., 2018)

Richard et al. (2020) developed a methodology for BESS optimal sizing in MATLAB/Simulink environment called SPIDER. This platform was developed by the French Alternative Energies and Atomic Energy Commission (CEA) and has several advantages, such as a graphic-modeling environment, high level of modularity, existing library of energy component models, templates, and ability to simulate different time steps (Richard, Pivert and Bourien, 2020). This sizing tool enables specification of a range of BESS size configurations and using the automatic processing, it is possible to find out which configuration size has the best outcome performance value.

From the sensitivity study results, the authors strongly recommend clearly defining a control strategy, taking aging into account, and that 10 min time-step instead of 1 hour time-step should be preferred in the optimization process. The importance of the correct control

strategy was demonstrated, where basic and advanced control strategies were compared. The outcome based on LCOE values suggested, that while LCOE for basic control strategy was the lowest for 444 kWh BESS energy capacity, for its advanced counterpart, the lowest value was for 333 kWh BESS energy capacity, which is a significant difference (Richard, Pivert and Bourien, 2020).

2.4.4 Mathematical approaches

Under this category, the size optimization can be expressed as linear programming, mixed-integer programming, or non-linear programming. To obtain the result from these methods, firstly an objective function is formed, which is then subjected to an iterative process until the best outcome is reached. Classical numerical methods may also be applied to solve optimization problems, such as gradient descending algorithm, interior point algorithm, or Newton's method. These provide certain advantages, including reduced computational load and limiting the number of steps needed to obtain results. Professional softwares like MATLAB and General Algebraic Modelling Systems (GAMS) are also available to solve optimization problems (Yang *et al.*, 2018).

2.4.5 Heuristics approaches

This category includes nature-inspired algorithms, which permit nonideal arrangements that are suitable for real-time applications. Some algorithms that can be utilized for BESS size optimization are genetic algorithm (GA), PSO, Tabu, or Bat Algorithms (Yang *et al.*, 2018) (Hannan *et al.*, 2021). The strengths of these approaches include fast convergence, solid adaptability, and straightforward execution to name a few (Hannan *et al.*, 2021). One of the most prominent algorithms mentioned in the literature for BESS size optimization is the genetic algorithm.

2.4.6 Optimization objectives

When optimizing for the size of the BESS, it is crucial to clearly define optimization objectives. Across the literature, the following are the most prevalent (Hannan *et al.*, 2021):

- cost - The objective is to reach the highest possible income while minimizing the overall cost of the system including the installation and operation costs (CAPEX and OPEX). The capital cost/expenditure (CAPEX) can include costs for battery pack, power conversion system, balance system, energy management system, engineering, procurement, and construction, developer overheads, grid connection, developer margin (Asian Development Bank, 2018). OPEX costs include operation (monitoring, repairs, data management), environmental checks (vegetation, waste management, safe battery disposal), security of the system (vandalism, theft, etc.), transmission-line control (regular checks and repair work), and spare parts (Asian Development Bank, 2018). Richard et al. suggest using Levelized Cost of Energy (LCOE) in [EUR/MWh] for a standalone system for estimation of the average cost of the energy, and Net Present Value (NPV) or Internal Rate of Return (IRR) for grid-connected systems due to variable feed-in tariffs, remuneration of ancillary services,

etc. (Richard, Pivert and Bourien, 2020). LCOE determines the average net present costs for energy production for the lifetime of the BESS and includes CAPEX, OPEX, energy generated in one year, discount rate, and lifetime of the system. NPV sets the present value of all future cash flows produced by the system, including CAPEX costs. The calculation variables include cashflow in a year, discount rate, and lifetime of the system. IRR is connected to NPV and is described as a discount rate that results in NPV being zero. The calculation includes the same variables as NPV with exception for discount rate which is replaced with IRR (Richard, Pivert and Bourien, 2020).

- capacity - Optimizing considers the storage capacity of the battery (MWh) and nominal power rating of battery converter (MW), thus optimizing the MWh/MW (storage/power) ratio.
- grid-connection power rating - when connecting a power generation unit (such as solar PV farm) into a distribution network, the most "unfavorable" effect is usually considered. This means that the maximum possible power injection is usually considered to be the power rating of PV inverter, even though the PV park produces the maximum power only a fraction of the time, resulting in the grid connection point being significantly oversized. With the BESS converter able to regulate the power output, it can lower the grid-connection power rating and thus allow more power generating units to be connected to the grid or just reduce the costs grid-connection points (Tejero-Gómez and Bayod-Rújula, 2023).
- lifetime - The lifetime of the battery is dependent on operation procedure, temperature, cell structure, and charge/discharge cycle. Various techniques have been employed to optimize the lifetime and it is occasionally coupled with a cost function (the longer the lifetime, the less frequent investment into a new battery). As an example for lifetime optimization, Badeda et al. (2017) strived to allocate battery power and capacity according to the state of health. The operation of the system adapts over the whole lifetime of the battery according to the current status and historical data (Hannan *et al.*, 2021; Badeda et al., 2017).

Optimization constraints are to be considered as well as they are considered to be prohibitive criteria. Defining their scope is often challenging as they are influenced by multiple factors including the surface area of the installation (footprint), climate, existing power grid infrastructure, or population (load demand). The most frequent system constraints are charging/discharging, battery capacity, environmental, and reliability (power and energy limits, defining BESS operation, defining SOC limits) (Hannan *et al.*, 2021).

Despite the increased effort to study BESS, the need for further research in size optimization and BESS incorporation with RES has been highlighted in various sources (Hannan *et al.*, 2021) (Das *et al.*, 2018). As already mentioned, Richard et al. (2020) have pointed out in their sensitivity analysis the importance of defining the control strategy in BESS size optimization. The basic model algorithm developed by Borkowski et al. (2023) strived to maximize the daily market revenue and was implemented using an analytical method based on irradiation and energy price data. The BESS was in this case coupled with a 1 MW solar

park and due to the large overlap of objectives, this work is largely based on the concept from this research. More specifically, the concept behind the basic control mode, together with the listed equations and conditions was applied. There have been identified uncertainties in the article, including the assumptions and the algorithm as only a flowchart was provided, and thus there was a need for adjustment and the resulting model from this work deviates from the original base concept (Borkowski, Oramus and Brzezinka, 2023). The procedure, as well as the base concept, is described in detail in the methodology.

The work by Tejero-Gómez and Bayond-Rújula (2023) argues that in the future with high solar energy penetration, the ability to provide constant power can become a crucial service. Their focus lies on guaranteeing a set power supply with a probability higher than 95%. The set point varies each month of the year and is based on an extensive data analysis. One of their main indicators for optimal sizing is a parameter called energy deficit (ED) which quantifies the the unavailability of energy in the system. The objective is to keep the annual energy deficit below 5% which ensures a firm power delivery to the grid. It must be noted that the authors did not consider any cost objective as they argued that in the future, the cost of the BESS will not be a limiting factor to the installation of the system (Tejero-Gómez and Bayod-Rújula, 2023). According to NREL, the capital costs (CAPEX) should reduce by 28-58% by 2030 and 28-75% by year 2050 compared to the prices published in 2019. They suspect the decline in the operation and maintance costs (OPEX) as well (Cole, Frazier and Augustine, 2021). To provide a comprehensive analysis of the optimal BESS sizing, this work was adapted as a comparison to the study by Borkowski et al. (2023) and is described in the Methodology.

3 Methodology

In this chapter, materials and methods used for analysis in this thesis work are outlined. First, the foundation research papers upon which the work is built are described, followed by the description of the Matlab model developed by the authors of this thesis. Modifications or improvements made from foundation papers are also outlined. Finally, the different spot price profiles used in simulations are explained.

3.1 The foundation concept for energy shifting - work by Borkowski et al. (2023)

The main concept behind the basic model developed by Borkowski et al. is to inject the energy into the grid in a way that maximizes the daily profit of the system. This was done by injecting part of the energy into the grid or sending it to the battery to be sent to the grid at a more appropriate time to take advantage of the price difference. The concept also allows for storing a fraction of generated energy when the energy from solar farm is higher than the rated nominal power of the system. The stored energy is discharged the next day during the highest price intervals. As already mentioned, the energy comes from a solar park connected to the BESS and the grid in the topology shown below (Borkowski, Oramus and Brzezinka,

2023). Their work is described in this subchapter followed by the adjustment made by the authors of this thesis.

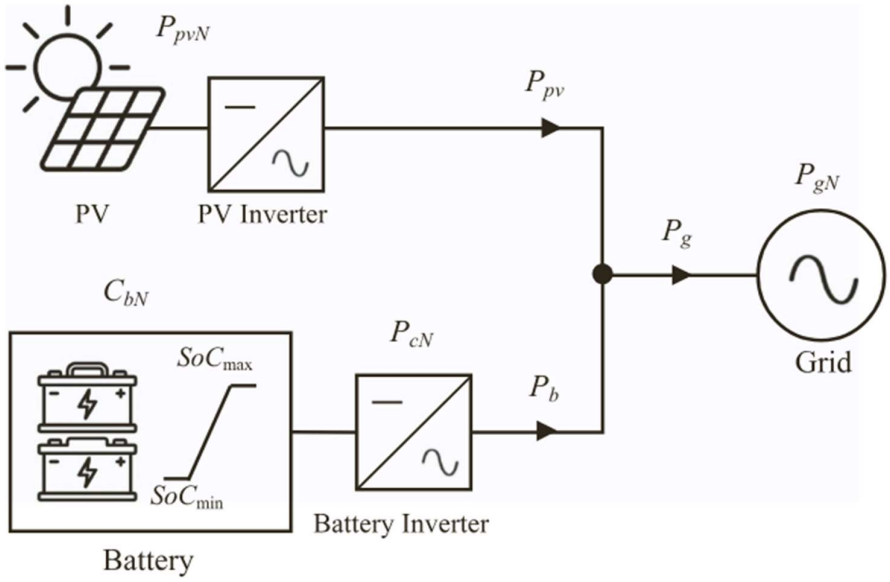

Figure 10 PV-BESS topology (Borkowski, Oramus and Brzezinka, 2023)

The authors identified several system constraints:

- system power balance, where $P_g(t) = P_{pv}(t) + P_b(t)$
- BESS power limitation, where $-P_cN \leq P_b(t) \leq P_cN$
- BESS SoC limitation, where $SOC_{min} \leq SOC(t) \leq SOC_{max}$
- power limitation of the grid, where $-P_gN \leq P_g(t) \leq P_gN$

The main optimization objective was cost efficiency using energy shifting. This would also allow an increase in installed PV capacity while retaining the same grid connection power rating (Borkowski, Oramus and Brzezinka, 2023). The flowchart for the algorithm used in the control strategy is shown below. The limitation of this system includes no energy trading (buying energy from the grid at lower price and discharging at higher price). The methodology used in this work is thus limited to the basic model described in Borkowki et al. (2023). On top of that, this simulation is based on the known solar irradiation and spot price data in order to be able to approximate the storage/power ratio. It was not in the scope of this work to create a control strategy for real-time energy production but rather base the approximations on the historical data.

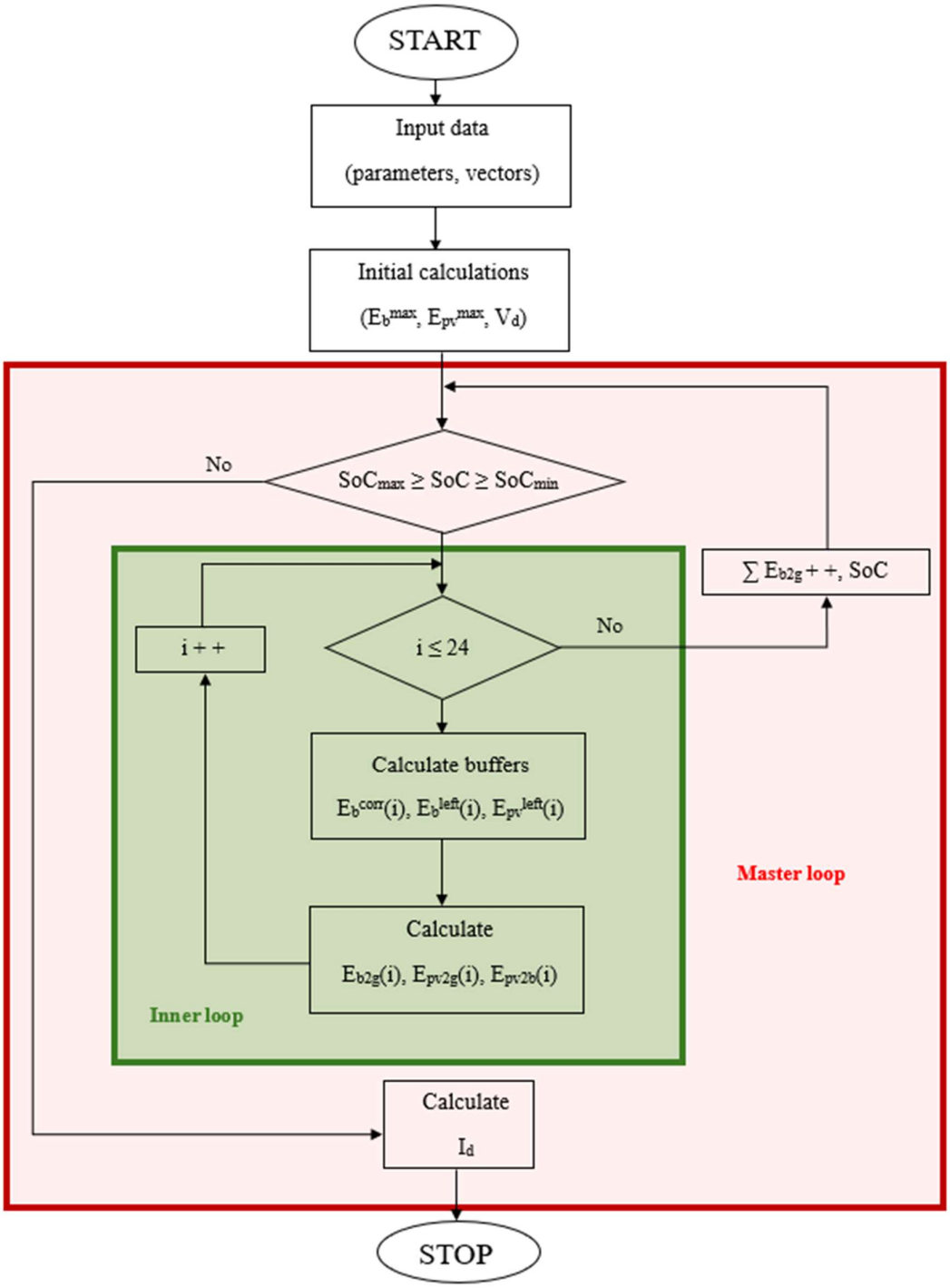

Figure 11 Flowchart for the basic model algorithm (Borkowski, Oramus and Brzezinka, 2023)

The input data include SOC_{min}, SOC_{max}, SOC, battery efficiency η_b, battery nominal capacityC_bN, nominal power of battery inverter P_cN, and nominal power of the system P_gN. The solar and price data are in the form of 24-element vectors, representing daily data on an hourly resolution.

After the data input, initial calculations are executed. The authors state in the text that all algorithm calculations are performed by Matlab software but do not specify whether Simulink or Stateflow environment was used (Borkowski, Oramus and Brzezinka, 2023).

The initial calculations are calculated at the beginning of the algorithm. Their calculation is explained as follows (Borkowski, Oramus and Brzezinka, 2023):

- E_b^{max} - maximum energy from solar PV park that can be stored in the battery, limited by the battery inverter power rating (P_cN)
- E_{pv}^{max} - maximum energy from solar PV park that can be sent to the grid and battery, limited by the power rating of battery inverted P_cN, and system power rating P_gN
- V_d - decision vector prioritizes hours of the day based on the modifier function (f_m) and price vector ($Price$), and is calculated as follows:

$$V_d = f_m . Price$$

the formula for the modifier function is given in the figure:

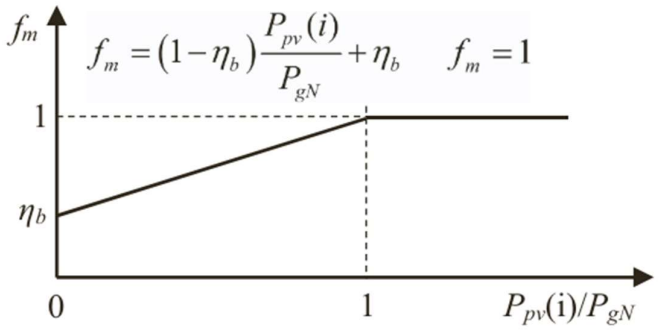

Figure 12 The modifier function (Borkowski, Oramus and Brzezinka, 2023)

The decision vector could be considered an essential part of the algorithm as it maximizes the return of the daily energy to the system determined by the hourly redistribution. The decision vector prioritizes hours based on price and modifier function, while the modifier function reduces the priority of hours if the solar production is less than the nominal power of the system (P_gN). After the calculation of the decision vector, it is then sorted in descending order. This determined the order of individual hours in which the energy is allocated. After the initial calculations, the simulation enters the master and inner loop (Borkowski, Oramus and Brzezinka, 2023).

The role of the master loop is to check the amount of energy that can be sent from the battery to the grid without exceeding the limit and check the SOC. The inner loop recalculated the daily energy based on the decision vector order. When solar energy is available, the priority is given to discharge to the grid. If the solar energy production from the solar park is lower than the system rating (P_gN), the energy is topped up from the battery (E_{b2g}) if possible (Borkowski, Oramus and Brzezinka, 2023).

The simulation first checks the number of hours in the day ($i = 1 \ldots . 24$) and then proceeds to calculate the so-called "buffers", which include $E_b^{corr}(i)$, $E_b^{left}(i)$, and $E_{pv}^{left}(i)$. The equations for these variables are given in the article and are defined as follows (Borkowski, Oramus and Brzezinka, 2023):

$$E_{b2g}(i) = \begin{cases} P_g N \,.\, T_s(i) & for \quad P_{pv}(i) < P_g N \\ 0 & for \quad P_{pv}(i) \geq P_g N \end{cases}$$

$E_{b2g}(i)$ is also limited by E_b^{left} and the battery inverter ($P_c N \,.\, T_s$). The E_b^{left} is an energy buffer and is defined as the amount of daily energy that can be obtained from the battery and is updated every hour. At the beginning of the day, the value of E_b^{left} equals the value of E_b^{max}(Borkowski, Oramus and Brzezinka, 2023). This value (E_b^{max}) is the amount of produced solar energy that can be stored in the battery each day and is limited by the nominal power rating of battery converter ($P_c N$). The equation and illustration are given below.

$$E_b^{left}(i) = E_b^{left}(i-1) - \frac{E_{b2g}(i)}{\eta_b} - E_{bcorr}(i)$$
$$E_b^{left}(0) = E_b^{max}$$

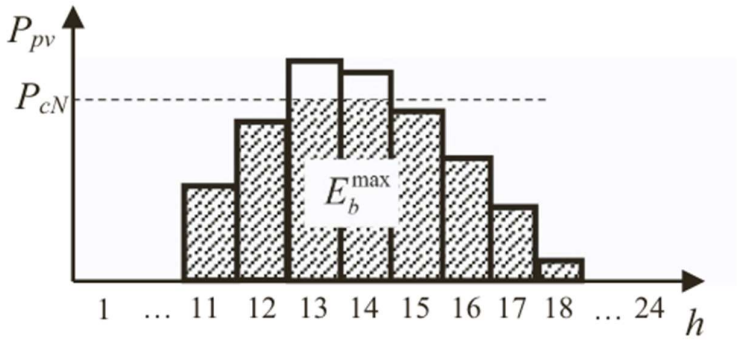

Figure 13 Illustration of E_b^{max} (Borkowski, Oramus and Brzezinka, 2023)

Next, E_{pv}^{left}, the PV energy buffer, is calculated. It is the amount of daily energy that can be sent to the battery and grid, updated every hour. At the beginning of the day, E_{pv}^{left} equals the value of E_{pv}^{max}. Similarly to E_b^{left}, E_{pv}^{left} sets a limit for E_{pv2g}, with another limit being the nominal power of the system ($P_g N \,.\, T_s$) (Borkowski, Oramus and Brzezinka, 2023). The equation and illustrations are given below.

$$E_{pv}^{left}(i) = E_{pv}^{left}(i-1) - E_{pv2g}(i) - \frac{E_{b2g}(i)}{\eta_b}$$
$$E_{pv}^{left}(0) = E_{pv}^{max}$$

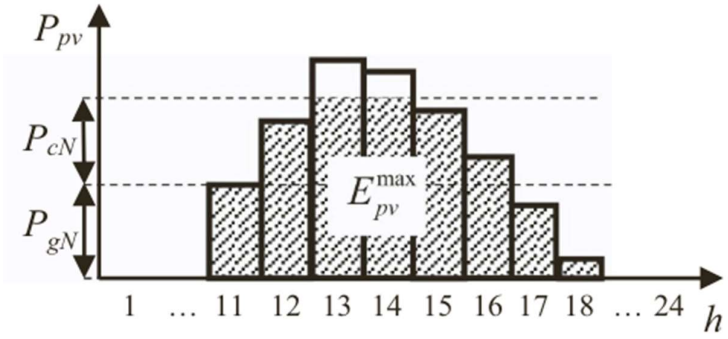

Figure 14 Illustration of E_{pv}^{max} (Borkowski, Oramus and Brzezinka, 2023)

Finally, $E_{bcorr}(i)$ is defined and serves the purpose of correcting the value of $E_b^{left}(i)$. It considers the solar energy sent to the grid in the previous step and is dependent on various scenarios (Borkowski, Oramus and Brzezinka, 2023):

$$E_{bcorr}(i) = \begin{cases} E_{pv2} & for \quad P_{pv} \leq P_cN \\ E_{pv2g} - E_{pv} + P_cN \,.\, T_s & for \quad else \\ 0 & for \quad P_{pv} \geq P_cN + P_{pv2g} \end{cases}$$

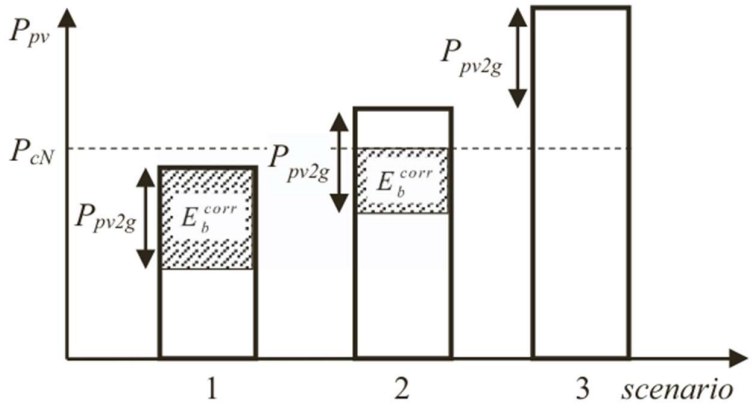

Figure 15 Illustration of E_{bcorr} (Borkowski, Oramus and Brzezinka, 2023

The last defined element in terms of energy redistribution is $E_{pv2b}\,(i)$, energy sent from the solar PV park to the battery and is dependent on two conditions (Borkowski, Oramus and Brzezinka, 2023):

$$Epv2b(i) = \begin{cases} (P_cN + P_gN)\,.\,T_s - E_{pv2g}(i) & for \quad P_{pv}\,(i) \geq P_cN + P_gN \\ E_{pv}(i) - E_{pv2g}(i) & for \quad else \end{cases}$$

At the end of the day and as a part of a master loop, income is calculated according to the following formula (Borkowski, Oramus and Brzezinka, 2023):

$$I_d = \sum_{i=1}^{24}((Epv2g(i) + Eb2g(i)).Price(i))$$

The following is the process summed up into the main steps:

1. 24-element vectors for daily solar energy and spot prices are obtained.
2. The decision vector is calculated based on spot prices and the modifier function which prioritizes the hours of high solar irradiation (higher or the equal to nominal power of the system).
3. Once the decision vector is calculated, it is then sorted in descending order. Based on the decision vector, the solar energy vector and spot price vector are reorganized. This results in the 24-element spot price vector being reorganized in such a way that the highest prices are moved to the beginning of the vector while the low prices are sorted to the back. This resorting helps redistribute energy based on the highest profit. The simulation reiterates through the individual elements of the vector, and it makes sure that the energy from the battery is primarily sent to the hours of the highest price. The redistribution is visualized in the Data processing subchapter in figures 22 and 23.
4. Maximum energy that can be sent to the battery and to the grid is calculated for a system to know how much energy can be redistributed.
5. After this, the inner loop is entered and iterates for 24 hours. In this inner loop, each hour the simulation decides whether to send energy to the grid, to the battery, or in case of low solar irradiation from the battery to the grid.
6. After 24 hours, the simulation leaves the inner loop and enters the master loop. Here the simulation calculates SOC and daily income from energy sent to the grid.

Now, it must be noted that the aforementioned study was taken as a base for the model developed in this thesis. However, the model deviates from the original concept due to needed adjustments, a lack of explanation, or incomplete information. The model development is described in the following subchapter.

3.2 The model development

The model was developed in the MATLAB software. For initial calculations, MATLAB Live script was used. The master and inner loop were initially developed in the Simulink and Stateflow environment, but later MATLAB Live Script was used to decrease the simulation time.

3.2.1 Data acquisition and processing

Firstly, data for solar irradiation and electricity spot prices were obtained. The reference points were chosen to be Trelleborg, Nörrköping, Umeå, and Kiruna in Sweden to provide solar irradiation data for all four price regions - SE1, SE2, SE3, and SE4.

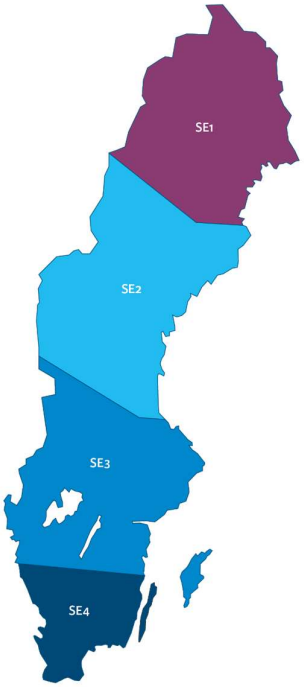

Figure 16 Electricity regions in Sweden (How does the electricity market work?, Tekniska verken)

The price data were obtained from the Energi Data Service developed by Energinet (Energinet, www.energidataservice.dk) and Fraunhofer Institute for Solar Energy Systems (*Spot Market Prices | Energy-Charts*). Yearly data for 2023 on the hourly resolution for all regions were generated and exported to .csv format. The spot price was given in EUR/MWh. The data was reorganized into an 8736x24 matrix.

The solar energy data was sourced from the Photovoltaic Geographical Information System developed by the European Commission (*JRC Photovoltaic Geographical Information System (PVGIS) - European Commission*). The data was taken from the "Average Daily Irradiance Data", from the PVGIS-SARAH2 solar radiation database for each month of the year on a slope suggested by the tool and azimuth 0°. The time chosen was UTC. The data was exported to .cvs format. The solar irradiation was given in W/m^2.

The model works on an hourly time step, and the data provided by the JRC PVGIS included only a 24-hour average daily data for a daily month. This was solved by replicating the average daily data for the total number of days in each month (31 days in January, 28 days in February, etc.). This is, of course, a rough estimation but due to the lack of data was deemed still representative enough for the calculations. A total of 8736 values was obtained (not 8760 due to the price data having only 8736). The data was reorganized in a 364x24 matrix.

3.2.2 Input data

The input data is the same as in the work by Borkowski et al. (2023) with some changes in the size. The system parameters remain the same: SOC_{init}, SOC_{min}, SOC_{max}, η_b, battery

nominal capacity C_bN, power rating of battery inverter P_cN, and system nominal power rating P_gN. Due to the optimization of C_bN and P_cN, these parameters vary in each size combination. The time step (T_s) is set to 1 h and remains constant The State of Charge parameters are calculated as given below:

$$SOC_{init} = 0.5 \,.\, C_bN \; [MWh]$$
$$SOC_{min} = 0.2 \,.\, C_bN \; [MWh]$$
$$SOC_{max} = 0.8 \,.\, C_bN \; [MWh]$$

Due to the calculations in the master and inner loop, these values were given in MWh, rather than percentage. The lifetime of a battery was assumed to be 10 years (timeframe used by Borkowski et al. (2023).

The solar irradiation data needed to be converted from the power given by W/m^2 into energy in MWh. To approximate the size needed for a 10 MW solar park at a location, the average size of the commercial solar panels (400 W) was used, with the following measurements:
width: 99 cm
length: 195 cm (A Guide to Solar Panel Sizes, Dimensions & Wattages in the UK).
To obtain the total number of solar panels, the power rating of the solar park (10 MW) was divided by the power rating of a solar panel, according to the following equation:

Number of solar panels = $P_{pv}N$ [W] / $P_{solar\ panels}$ [W]
Number of solar panels = $10.10^6 \,/\, 400 \;=\; 25\,000$

The needed area was calculated using the number of solar panels and their measurements.

Area = Width [m] . Length [m] . Number of solar panels
Area = $99/100 \,.\, 195/100 \,.\, 25\,000 \;=\; 48\,262.5\ m^2$

With total area, it was possible to estimate total energy production from solar farm. To calculate the resulting energy, solar panel efficiency (20%), and power components efficiency (90%) needed to be taken into account (*Photovoltaic Energy Factsheet*, Center For Sustainable Systems; *6.5. Efficiency of Inverters | EME 812: Utility Solar Power and Concentration*, PennState).

Then solar energy corresponding for one hour can be calculated accordingly:

$$Solar\ energy \;=\; (P(i) \,.\, A \,.\, \eta_{solar\ panels} \,.\, \eta_{power\ components} . Ts) \,/\, 10^6 \;\; [MWh]$$

where:
P(i) - power from solar park on an hourly basis [W/m2]
A - area of the solar park [m2]
$\eta_{solar\ panels}$ - efficiency of solar panels
$\eta_{power\ components}$ - efficiency of power components

Ts - time step (1h)

As the price data was already given in EUR/MWh, there was no need for conversion.

3.2.3 Initial calculations

In the initial calculations, E_b^{max}, E_{pv}^{max}, and V_d vectors were determined. The solar energy and price matrices were reorganized based on the decision vector and then were reshaped into 1x8736 vectors for simulation purposes.

The code for calculating E_b^{max} and E_{pv}^{max}:

```
% Initial calculations - Ebmax, Epvmax
% Calculation for Ebmax
PcN_limit = PcN;
limited_solar_energy_PcN = min(solar_energy, PcN_limit);
Ebmax = sum(limited_solar_energy_PcN,2);
Ebmax = Ebmax';

% Calculation for Epvmax
PgN_limit = PgN;
limited_solar_energy_PgN = min(solar_energy, PgN_limit);
Egmax = sum(limited_solar_energy_PgN,2);
Egmax = Egmax';
Epvmax = Ebmax + Egmax;
```

Next, the decision vector (V_d) was calculated and sorted in descending order. Solar energy and price (spot price) matrices were reorganized and reshaped according to this code:

```
% Calculation for decision vector Vd
fm = (1-efficiency_BESS).* (solar_energy/PgN) + efficiency_BESS; % modifier
function
Vd = fm .* spotprice;

% Incorporating the decision vector, sorting it into descending order
% Sorting Vd and getting the sorting indices
[sortedVd, sortOrder] = sort(Vd, 2, 'descend');

% Using the sorting indices to reorder solar energy and spot prices
sortedSolar_energy = zeros(size(solar_energy));
for i = 1:size(solar_energy, 1)
    sortedSolar_energy(i, :) = solar_energy(i, sortOrder(i, :));
end
irradiation_year = reshape(sortedSolar_energy', 1, []);

sortedspotprice = zeros(size(spotprice));
for i = 1:size(spotprice, 1)
    sortedspotprice(i, :) = spotprice(i, sortOrder(i, :));
end
```

```
sortedspotprice = reshape(sortedspotprice', 1, []);
```

3.2.4 Master and inner loop

As already mentioned, the model was initially developed in the Stateflow/Simulink environment according to work by Borkowski et al. (2023). The flowchart of the simulation used in this work is provided below. The calculation has been adjusted by adding the feature of storing energy from the solar park in the battery in the event of negative prices. To ensure the SOC was kept within the limits, each day the amount of available energy stored in the battery throughout the previous day was calculated and was one of the possible limits for E_b^{left} (min(Energy available, E_b^{max})). Moreover, energy was only stored in the battery if the addition did not violate the SOC limitations.

The objective of this optimization method was to maximize the profit of the BESS system. For that reason, the rate of return (RoR) was chosen as a financial indicator.

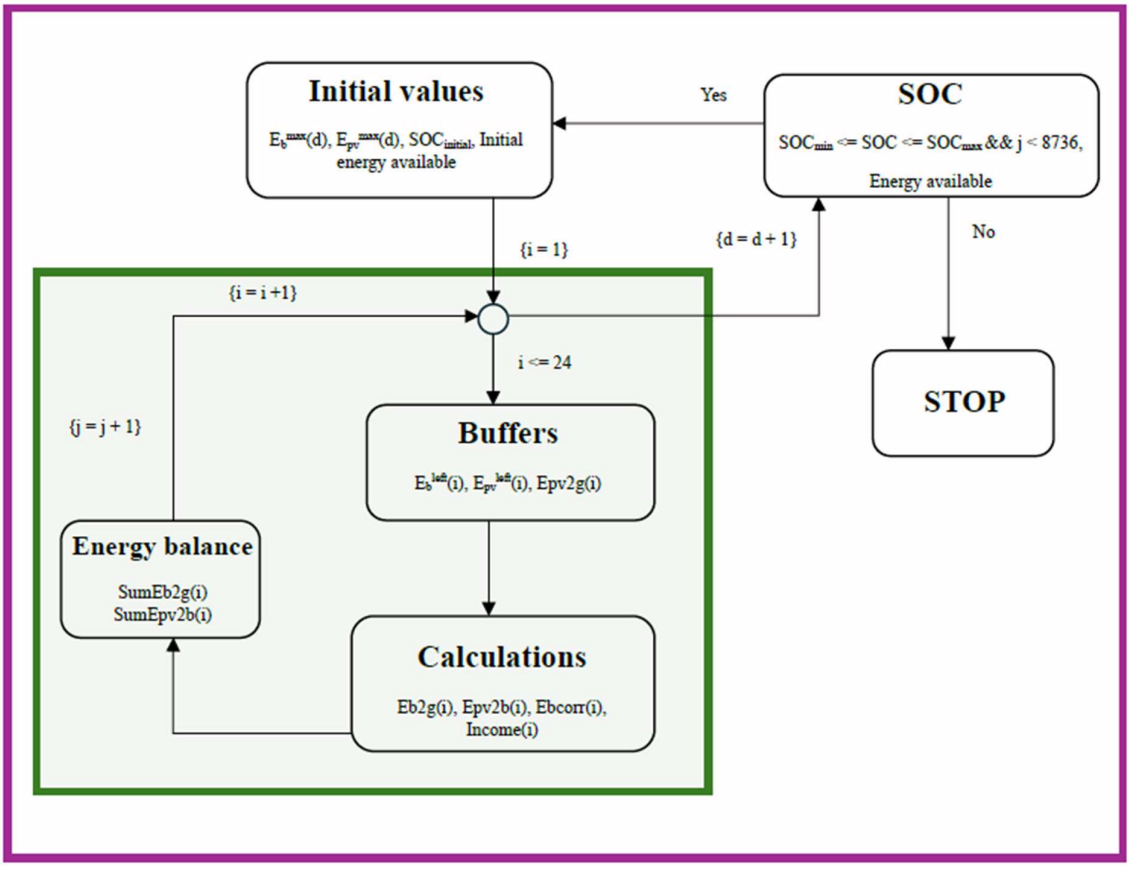

Figure 17 Simulation flowchart

The simulation code was later recreated in the MATLAB script due to the excessive simulation time. The total time required for running a one-year solar data in Stateflow was approximately 8 hours which significantly hindered the optimization process as it was

possible to evaluate only one set of size combinations at a time. After this, the simulation time was reduced to a few seconds.

A total of 620 combinations for all price areas (155 per price area) were evaluated.
C_bN values [MWh]: 5, 10, 15, 20, 25, 30, 35, 40, 45, 50, 55, 60, 70, 80
P_cN values [MW]: 0.5, 1, 1.5, 2, 2.5, 3, 4, 5, 7, 8, 9

$$P_gN = P_{pv}N + P_cN$$

The results of a yearly total income were multiplied by 10 years which was assumed to be the lifetime of the battery as done in Borkowski et al. (2023). Increasing lifetime affects battery capacity, which decreases with the number of cycles (4000 - 6000 for lithium-ion batteries) and the end of life is usually considered to be 80% of the former battery capacity (Borkowski, Oramus and Brzezinka, 2023). Instead of calculating the income at the end of the day as done by Borkowski et al. (2023), it was calculated every hour as Income(i) with the following equation:

$$Income(i) = ((Epv2g(i) + Eb2g(i)).Price(i))$$

The expenses were calculated using price data from the National Renewable Energy Laboratory (NREL) cost projections of energy components for Li-ion BESS for 2025.
Unit BESS power cost - $100/kW
Unit BESS capacity cost - $250/kWh (Cole, Frazier and Augustine, 2021).
The conversion rate as of 9.5.2024 (1:49 PM EDT) was $1.000 = 0.928 € (*USD to EUR Exchange Rate*, Bloomberg). After the conversion, the price in EUR:
Unit BESS power cost (Kc) - 93 EUR/kW
Unit BESS capacity cost (Kp) - 232 EUR/kWh

The total PV-BESS cost (K) and the RoR for each combination were calculated according to the formulas given by Borkowski et al. (2023):

$$K = K_c \,.C_bN + K_p \,.P_cN$$

$$RoR = \frac{\sum_{n=1}^{Ny} Iy - (K + Ke\,.Ny)}{K + Ke\,.Ny}.100\ [\%]$$

where Ke is the annual operation cost and was estimated to be $10/kW (9.28€/kW) (Mongird *et al.*, 2020), Ny is the number of operation years, and Iy is the income over the BESS lifetime.

The optimum BESS size was determined by the maximum RoR and no violations in terms of hourly SOC for each of the Swedish electricity network regions - SE1, SE2, SE3, SE4. The irradiation data used was from locations within the regions, the list provided below. The

optimum sizes (Capacity/Solar power rating) were applied to the solar parks depending on which region they belonged to.

Region - Irradiation data location
SE1 - Kiruna
SE2 - Umeå
SE3 - Norrköping
SE4 - Trelleborg

3.2.5 High solar energy penetration price profile

To evaluate the profitability of the BESS for energy shifting, a price profile for high solar energy penetration was developed. As shown in Borkowski et al. (2023) and in the figure below, the price profile is characterized by lower prices around noon compared to price profiles from 2021 and 2022 (Borkowski, Oramus and Brzezinka, 2023).

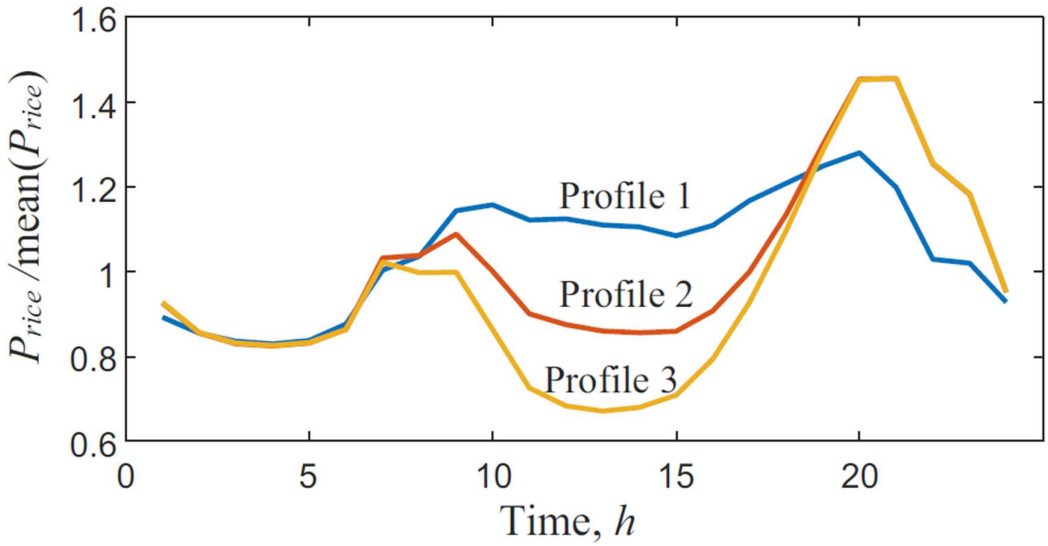

Figure 18 Price profiles (Borkowski, Oramus and Brzezinka, 2023)

The price profile for high solar penetration developed in this work is based on the SE4 price profile. Firstly, the yearly average, minimum, and maximum prices were found. The daily pattern was identified based on profile 3 by Borkowski et al. (2023) and is described below:

00:00 - 05:00 - average yearly prices
06:00 - 08:00 - interpolation between average and maximum yearly prices
08:00 - 09:00 - maximum yearly prices
09:00 - 11:00 - interpolation between maximum and minimum yearly prices
11:00 - 14:00 - minimum yearly prices
14:00 - 18:00 - interpolation between minimum and maximum yearly prices
18:00 - 19:00 - maximum yearly prices
19:00 - 22:00 - interpolation between maximum and average yearly prices
22:00 - 24:00 - average yearly prices

The daily pattern as described above was developed based on the high peak recorded in profile 3 by Borkowski et al. (2023). As can be seen, in the morning, the spot price does not rise as much in the price profile 3 but the Day-ahead price predictions from Nordpool in figure 19 show both morning and evening spot price peaks.

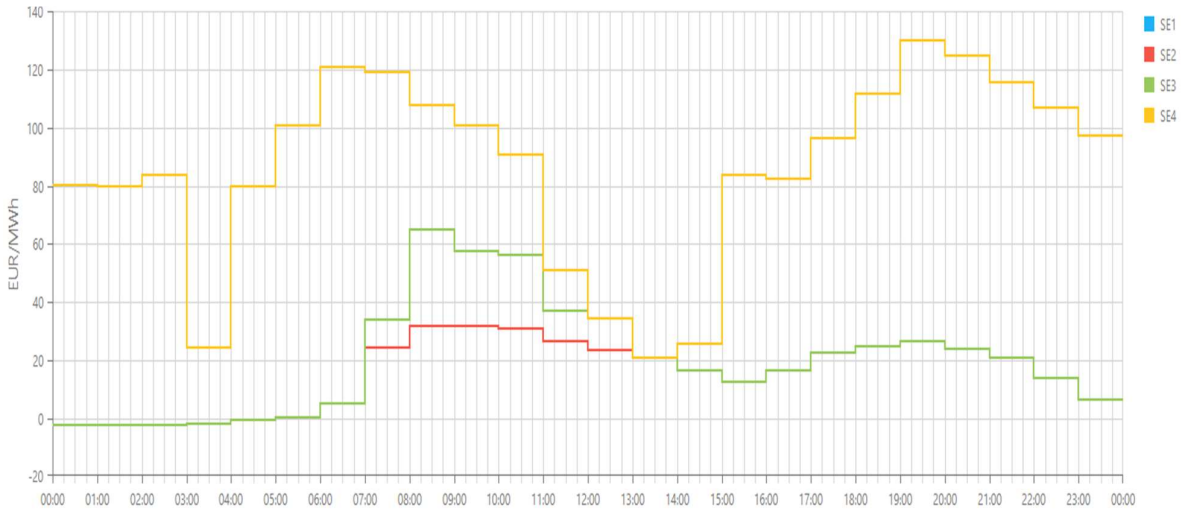

Figure 19 Day-ahead Prices from Nordpool for 24.5.2024 (Nord Pool | Day-ahead prices)

After this, the prices were normalized to the average yearly price resulting in the price profile shown below. The average price was then found for every day of the year and multiplied by the daily trend to obtain yearly price data at a given location. An example of this method is shown in figure 21.

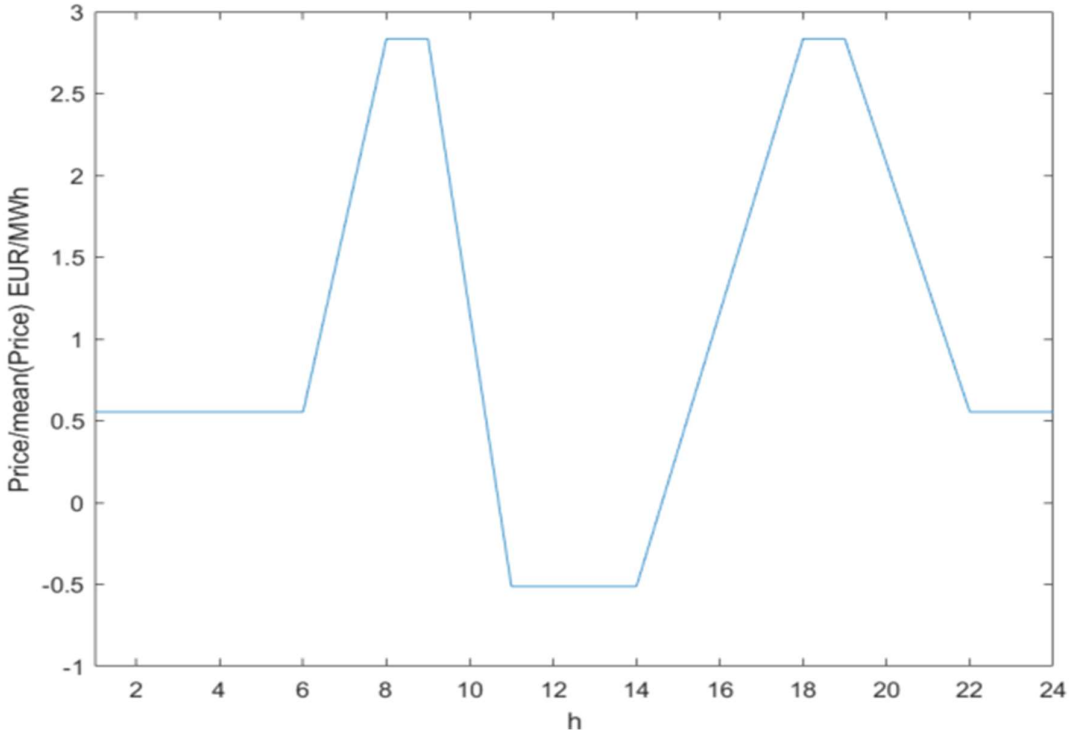

Figure 20 Price profile for high solar penetration

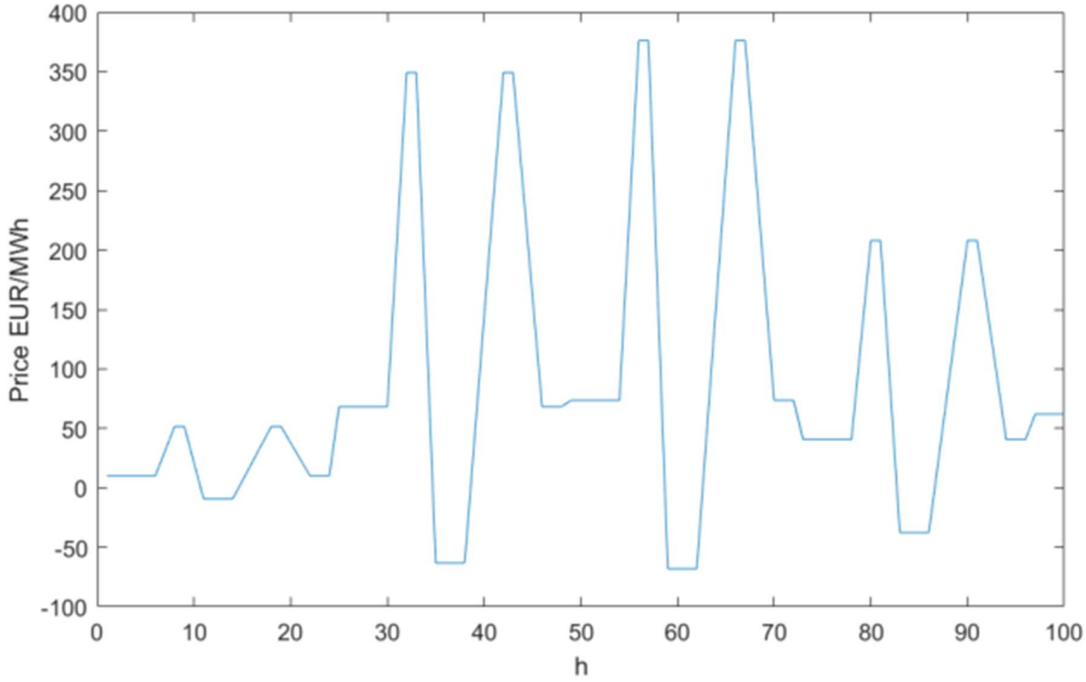

Figure 21 Price profile for high solar penetration, SE4 first 100 hours

3.2.6 Data processing

After the simulation, the data was sorted to its original format (before the decision vector resorting), processed, and visualized in MATLAB. The hourly SOC was calculated again

using the initial SOC (50%), $E_{pv2b}(i)$, and $E_{b2g}(i)$. The sorted and unsorted hourly energy balancing is shown in the figures below.

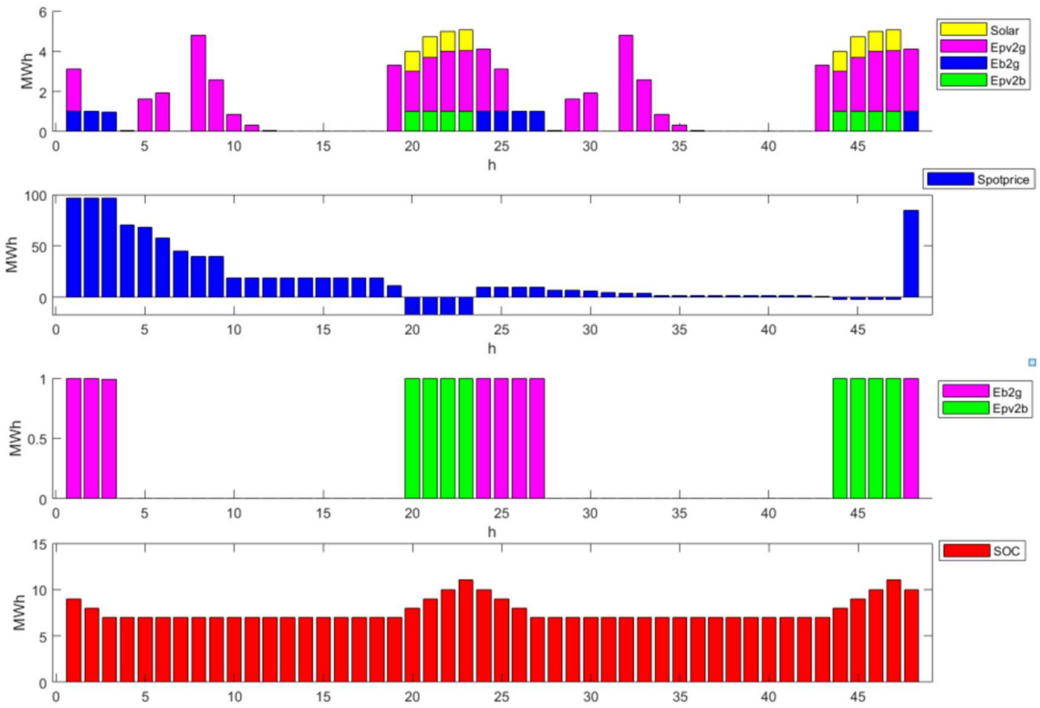

Figure 22 Unsorted energy balance results for high solar energy penetration price profile

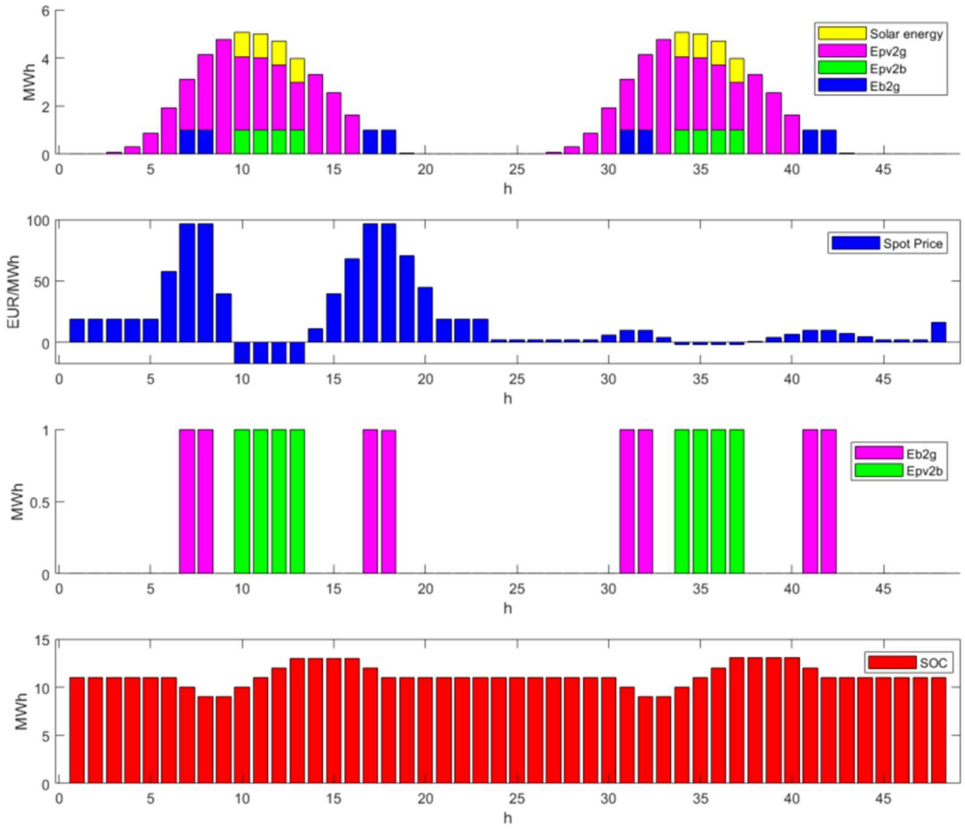

Figure 23 Sorted energy balance results for high solar energy penetration price profile

The list of solar parks above 1 MW located in Sweden was created. A total of 49 solar PV parks were found with a maximum power rating of 22 MW being Kungsåra Sollcelspark outside Västerås (*Anläggningar över 1 MW*, Svensk Solenergi; *Open Infrastructure Map*). The optimum size was calculated for each solar park to approximate the market size.

3.2.7 Main changes from the article by Borkowski et al. (2023)

The main changes include:

- adding the feature of storing solar energy in the battery in case of negative prices in the basic model,
- resorting the results back to the original format for further analysis and SOC check,
- adjusting the simulation code,
- the assumption that 1-year data are sufficiently representative of 10 years,
- SE1, SE2, SE3, and SE4 energy prices were utilized instead of price profiles,
- various irradiation locations were used (across Sweden),
- the aging (degradation) of the battery was not accounted for in this work, but rather the lifetime was assumed to be 10 years.

3.3 Monthly Constant Power Operation by Tejero-Gómez and Bayond-Rújula (2023)

To ensure a constant power supply to the grid, the authors strived to homogenize the hourly production of the solar park to be able to obtain the most optimal setpoint for each month. The figure below illustrates the concept behind the simulation - redistributing the solar energy (blue) into a constant level. The values are given in p.u. It would be possible to optimize the system for charging and discharging the stored energy according to the local load (e.g. production site), creating a system that is essentially a combination of energy shifting and constant power delivery. However, the scope of this work covered only the two separate services.

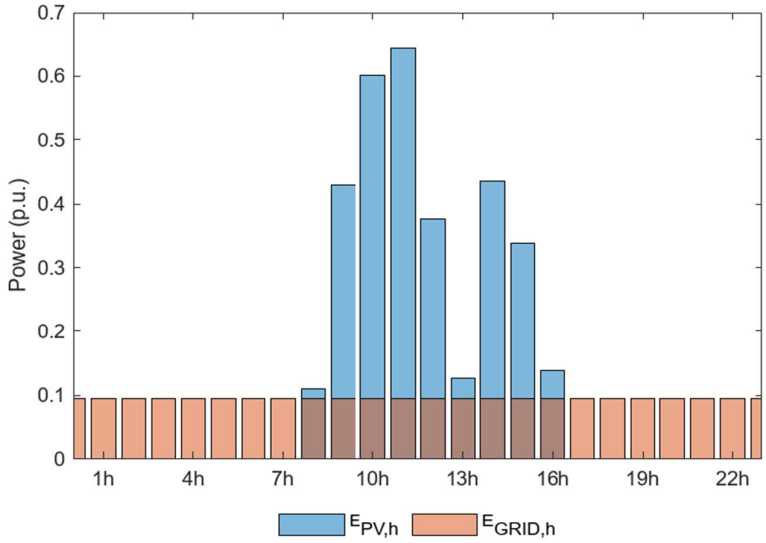

Figure 24 Redistribution of solar energy (Tejero-Gómez and Bayod-Rújula, 2023)

The studied PV-BESS topology matches that of the previous work by Borkowski et al. (2023) and is shown below.

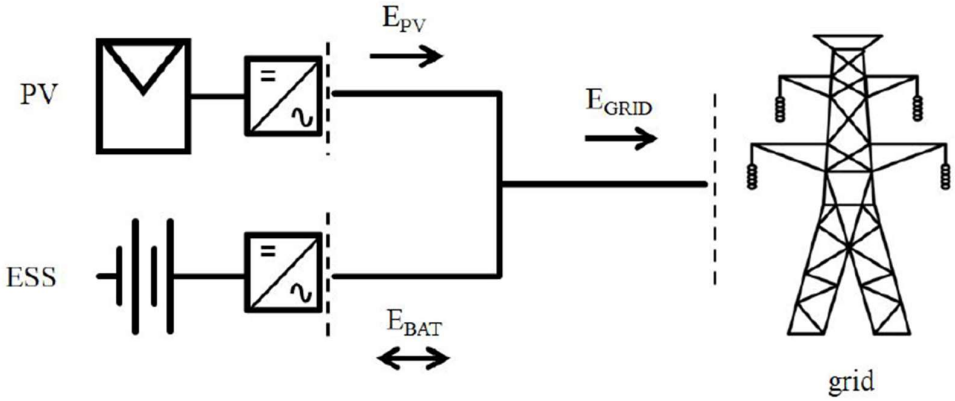

Figure 25 PV-BESS topology (Tejero-Gómez and Bayod-Rújula, 2023)

Due to time and resource limitations, the calculations were reduced to the level of estimation. The solar data analyzed was a maximum daily irradiation profile (the day of the year with the highest solar irradiation) as it was assumed that the highest possible storage capacity requirement would be during this time. The reference size of the solar park was set to 10 MW and the total area calculation was the same as in the previous method.

The main design parameter was the S2P ratio defined as a ratio of storage capacity to the nominal power rating (inverse of C-rate) of a solar farm calculated according to the formula given in Tejero-Gómez and Bayod-Rújula (2023):

$$S2P = \frac{C_{BESS}}{P_{PV}}$$

Contrary to the foundation concept, the value of $CPOf$ was set to 1. The authors of the article argued that the value of $CPOf$ should be less than the value of the capacity factor, CF, which is in the case of solar parks around 15 - 40 % (Tejero-Gómez and Bayod-Rújula, 2023). The formula is shown below:

$$CPOf = \frac{P_{GRID}}{P_{PV}}$$

However, in this work, it was assumed that the $P_{GRIDnominal}$ (constant power to be supplied to the network) should be equal to at least the average of the daily power generation. If this value was lower than 1, we might encounter the problem of not being able to output enough power and if it is greater than 1, we are essentially oversizing the system. Thus, the utilized equation for $P_{GRIDnominal}$ was as follows:

$$P_{GRIDnominal} = CPOf \,.mean(P_{PV})$$

The main loop simulation for daily irradiation data was based on ensuring constant power delivery to the grid. This was done by storing energy in case power from the solar park was higher than the rated power of the grid and discharging energy in the event of solar power being lower than the rated power of the grid. Storing and discharging of energy were also limited by the SOC minimum and maximum setpoints - 20% and 80% respectively.

The optimal S2P ratio was chosen based on the energy deficit value (ED) and SOC limits. This means that the size that maximized the battery utilization (SOC ranging from $SOC_{min}$to SOC_{max}), and at the same time minimized the ED was deemed to be the solution for a given location. The surplus energy (SP) was calculated as well, but as there are various options to utilize the extra energy, it was not viewed as the deciding factor in this method. The equations for ED and SP are provided below.

$$ED = ED + abs(P_{GRID}(i-1) - P_{GRIDnominal})$$
$$ED = ED/\,(24\,.P_{GRIDnominal})$$

$$SP = SP + abs(P_{GRID}(i-1) - P_{GRIDnominal})$$
$$SP = SP/(24 . P_{GRIDnominal})$$

where

$$P_{GRID}(i-1) = P_{PV}(i-1) + P_{BESS}(i-1)$$

service	foundation work	optimization objectives	evaluated price profiles	simulation time
energy shifting	Borkowski, Oramus and Brzezinka, 2023	rate of return (RoR), SoC	SE1, SE2, SE3, SE4, high solar energy penetration price profile	one year on hourly basis (8736 hours)

In this equation, P_{BESS} is the energy needed to be supplied/stored in the battery at the given hour.

After the simulation, the optimum S2P was determined for each price region, and the optimum storage size was calculated for all solar parks in the list. This provides a comparison of BESS size requirements based on two different services and gives deeper insight into the market size.

1.4 Summary of the methodology

The summary highlighting crucial aspects of the methodology is provided in the table below.

Table 2 Summary of the methodology

constant power delivery	Tejero-Gómez and Bayod-Rújula, 2023	energy deficit (ED), SoC	SE1, SE2, SE3, SE4	one day of the highest yearly irradiance (24 hours)

4 Results and Discussion

This chapter will present the results of the performance of the site-specific PV plants in Sweden using BESS for energy shifting and constant power application. First, the energy shifting and constant power BESS applications with their market size will be presented from the evaluation during conditions reassembling today's conditions. Followed by a section where the same application is evaluated during conditions created from future scenarios. The second part of the chapter presents an analysis of the differences and similarities between these sites.

4.1 BESS market size in Sweden

The BESS capacity needed for each solar PV farm in Sweden was evaluated based on the plant-installed power and ROR. To begin with, the 2023 spot price profile and solar irradiation at the optimal angle for four cities in four different price areas were evaluated. Figures 26 and 27 show the monthly solar irradiation for the four cities under consideration and the average solar distribution in Sweden.

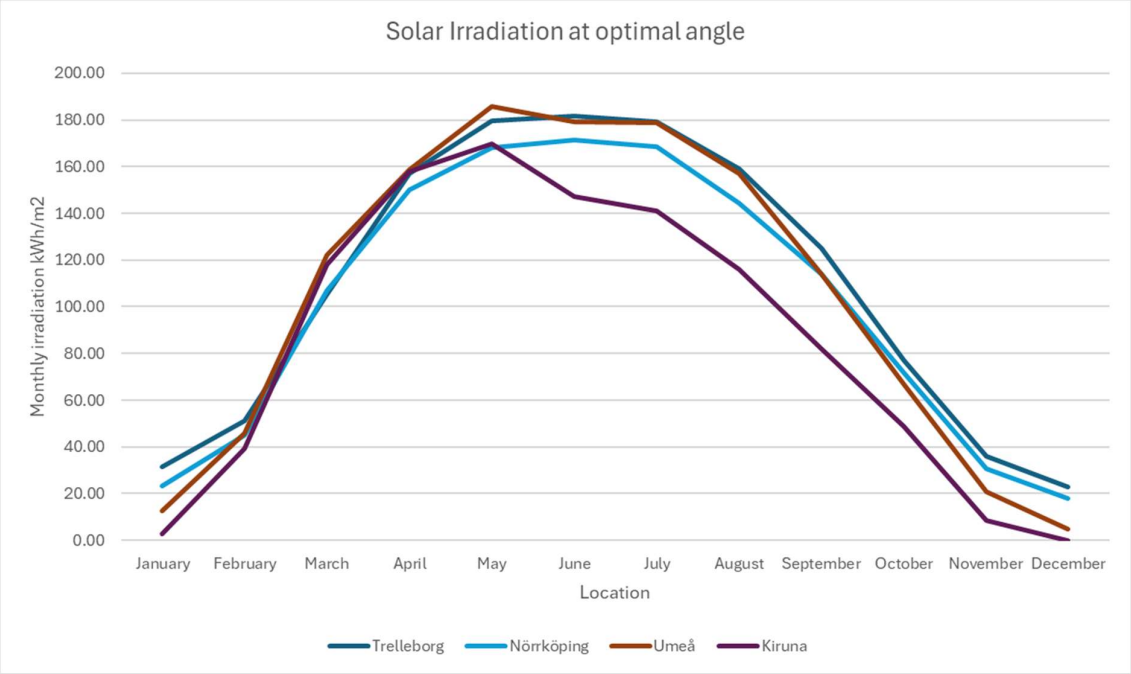

Figure 26 Monthly solar irradiation for the four cities in Sweden

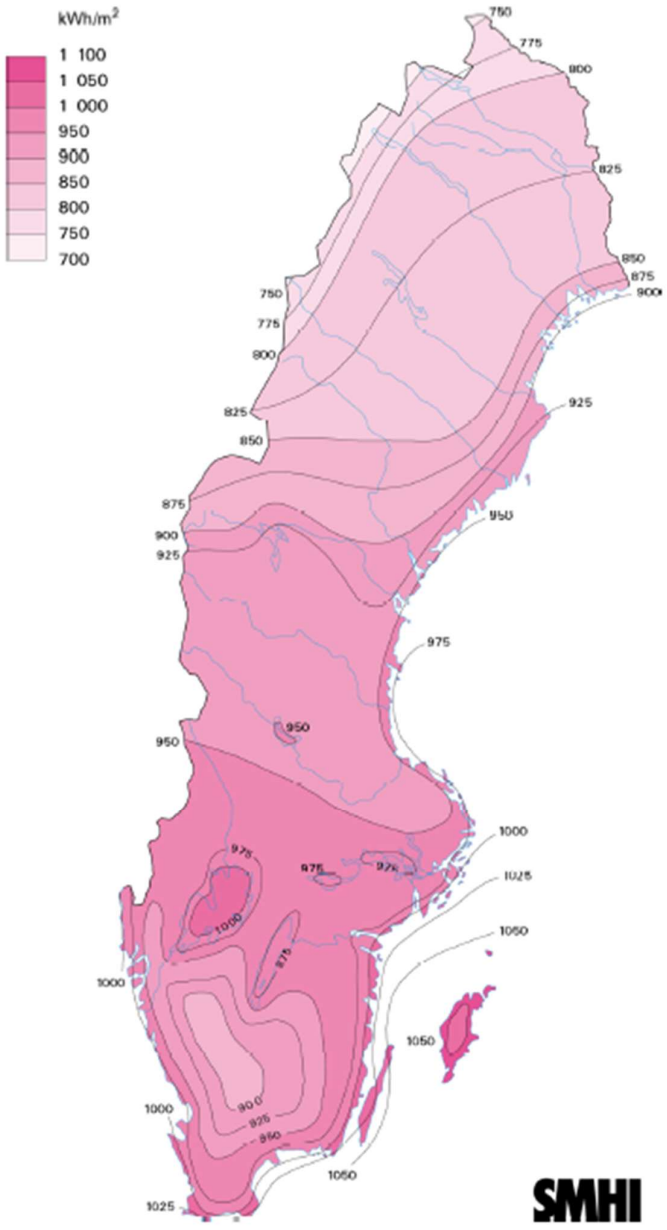

Figure 27 Global radiation for a whole year during the defined normal period 1961-1990 in Sweden (SMHI, 2024)

The economic analysis for optimized BESS installation for all the existing PV plants in Sweden was evaluated from the perspective of the ROR value. The current values for BESS CAPEX and OPEX, as stated in Table 3.

Table 3 Values used in BESS economic analysis

Parameter	**Value**	**Source**
Lifespan of BESS	10 year	(Borkowski, Oramus and Brzezinka, 2023)
CAPEX - Unit BESS power cost	$100/kW	(Cole, Frazier and Augustine, 2021)
CAPEX - Unit BESS capacity cost	$250/kWh	(Cole, Frazier and Augustine, 2021)
OPEX - Annual BESS operational cost	$10/kW	(Mongird *et al.*, 2020)

4.2 Spot price scenarios

This chapter presents and evaluates two different price profile scenarios to analyze the profitability of BESS installation in existing solar parks in Sweden.

1. Scenario 1: 2023 spot prices are characterized by large spot price fluctuations during the normal day. This scenario assumes an increase in the adoption of renewable sources as existing nuclear power plants are retired in Sweden. It assumes that there will be high spot price fluctuations throughout the day. In this scenario, spot prices are high before and after midday due to high demand when people go and come home after work. At night, the price will be lower due to reduced demand.

2. Scenario 2: The future scenario is characterized by high solar penetration of commercial PV farms and the spot prices are negative during the day and very high in the morning and evening when the irradiation is low. The difference between scenario 1 and scenario 2 is increased penetration of solar PV farms and change in the spot price daily profiles.

4.3 Energy shifting

4.3.1 Optimized BESS capacity in price areas - Scenario 1

To determine the optimized BESS capacity for price areas in Sweden suitable for energy shifting purposes based on the spot price and hours of high irradiation, two important aspects were considered;

1. Rate of Return (ROR): In order to ascertain if incorporating BESS to existing PV installation in Sweden price areas will result in a profit/loss during the lifespan of

BESS installation (assumed 10 years), the ROR parameter was used. Rates of return are normally expressed as percentages, which make it easier to compare the performance of different investments. Positive rates of return indicate growth or profit, while negative rates indicate loss or decline. In analyzing the obtained results, it should be noted that the spot price profile used in the simulation was based on the 2023 financial year. The spot price profile affects the ROR parameter due to variations in daily market revenue.

2. State of Charge (SOC): In order to make the best use of BESS and not violate the intended lifespan of the battery, it is important to operate the BESS within a manufacturer-recommended minimum and maximum SOC limits.

Figure 28 below shows the variation of ROR with increasing optimized BESS capacity in SE1 and SE2. The minimum required BESS capacity for the purposes of energy shifting is 20 MWh in both areas, with an ROR of -24.9% and -23.1% for SE1 and SE2, respectively, over a period of 10 years. The results suggest a loss in BESS investment to the customer in these regions, assuming the same spot price profile for 2023 and solar irradiation over the lifespan of the battery. As indicated in Table 4, the minimum converter power rating, P_cN, for both SE1 and SE2 is 0.5 MW.

In Figure 28, it is evident that extrapolating the ROR curve upwards towards the X-axis will result in smaller BESS capacities. However, the simulation results obtained showed that the smaller BESS capacities violated the SOC. Using smaller BESS capacities may be profitable for other BESS applications not covered by this thesis work.

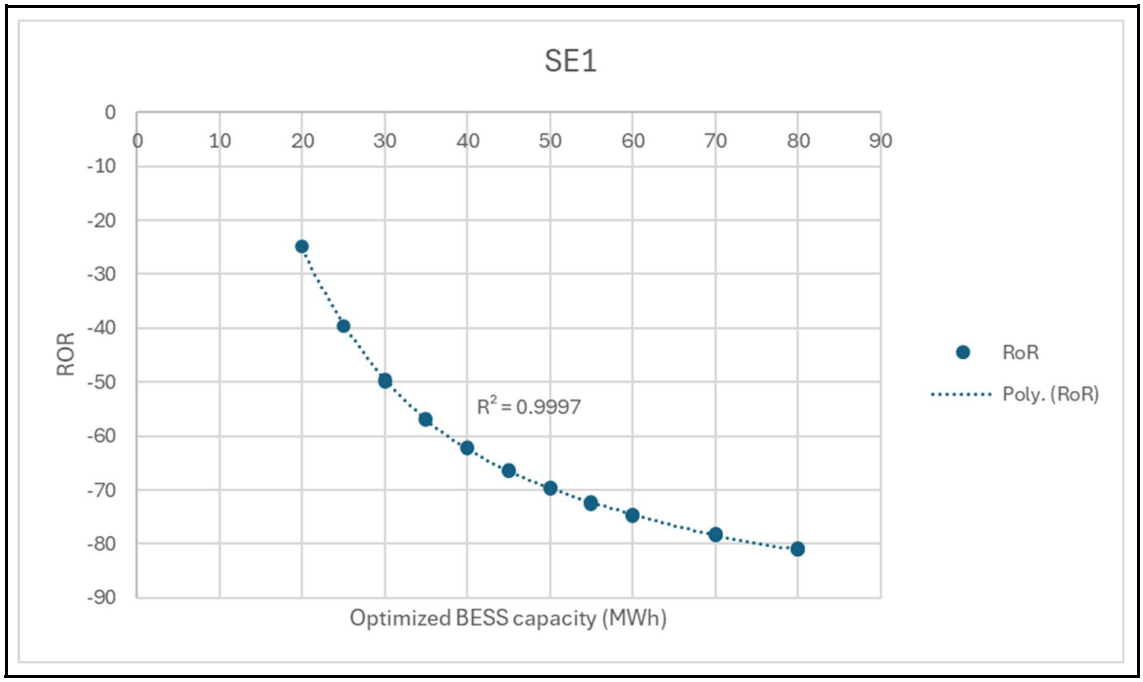

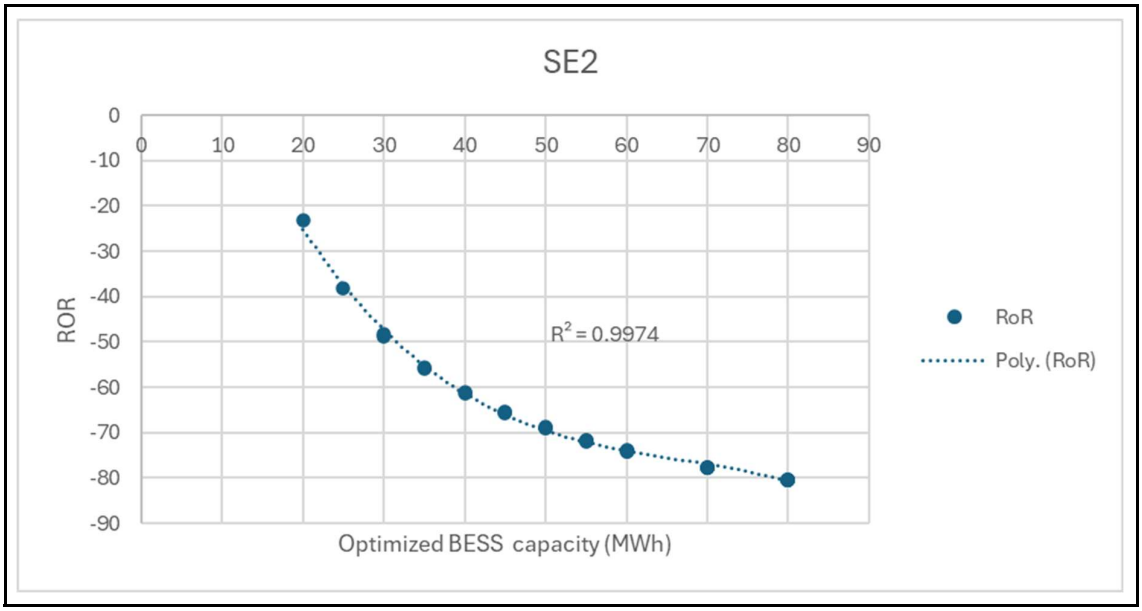

Figure 28 Scenario 1 - Comparison of ROR and optimized BESS capacity size in SE1 and SE2

The results in SE3 and SE4 are different from SE1 and SE2. In SE3, the BESS capacity of 5 MWh, 10 MWh, and 15 MWh yields a gain or profit on the investment. Conversely, a BESS capacity of 20 MWh is required in SE4. Increasing the BESS capacity beyond 15 MWh in SE3 and 23 MWh results in a negative ROR due to not having significant income compared to the initial BESS capital investment and incurred operational and maintenance costs during the lifespan of the installation.

The difference in the obtained results for SE1, SE2, SE3, and SE4 is mainly driven by the spot prices and the solar irradiation. The northern part of Sweden (SE1 and SE2) generates more electricity than what is consumed by customers. In southern Sweden it is the opposite. Therefore, large amounts of electricity is transmitted from the north to the south. Local imbalances in production and consumption are clearly visible. In 2021, the two northern bidding zones generated a significant electricity surplus of 51.5 TWh. The southern bidding zones (SE3 and SE4) had a combined electricity generation deficit of 26 TWh (Holmberg & Tangerås, 2023). Due to this deference in generation and consumption of electricity, the south of Sweden is characterized by higher spot prices compare to the northern part of the country.
The difference in the average solar irradiation between these price areas is another driven factor. As shown in Figure 27, Kiruna (SE1) has an average global irradiation of approximately 800 kW/m^2 compared to SE4 that has around 1050 kW/m^2. This explains why the ROR is positive in SE3 and SE4 but negative for SE1 and SE2.

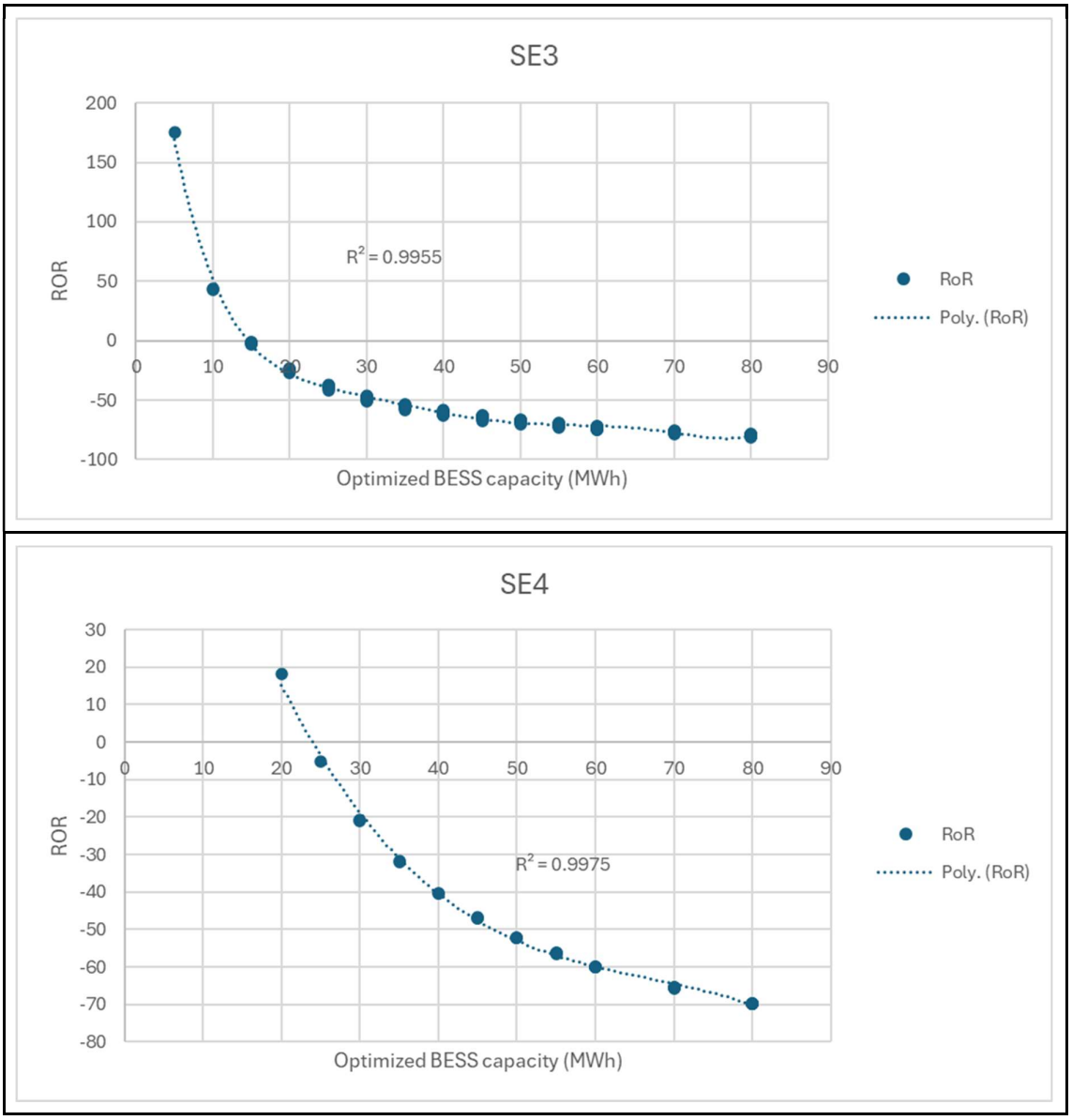

Figure 29 Scenario 1 - Comparison of ROR and optimized BESS capacity size in SE3 and SE4

In the energy sector, and specifically with regard to spot prices for electricity, geopolitical risks can have a significant effect. These hazards include occurrences or situations involving political unrest, hostilities, or other international problems that may affect the supply and demand for energy and cause price volatility. For example, a geopolitical event like a war, terrorist attack, or natural disaster can impact the availability of gas and oil, which are used in many nations to produce electricity. A shortage of electricity may result from disruptions in the oil and gas supply, and due to increased demand, prices may rise. Furthermore, the investment climate for renewable energy projects may be impacted by geopolitical risks, which could result in project cancellations or delays (Saâdaoui and Ben Jabeur, 2023). This is typified by scenario 1.

4.3.2 Optimized BESS capacity in price areas - Scenario 2

According to a thorough analysis by (López Prol, Steininger and Zilberman, 2020), there is pressure on electricity prices to decline as renewable technologies become more prevalent in the wholesale electricity markets. This has significant ramifications not only for the wholesale electricity market as a whole but also for policy makers. In order to have an insight into the impact of future spot prices, the scenario 2 profile was used to simulate the four price areas in Sweden with an assumption of future high solar penetration into the national grid.

Figure 30 below shows the variation of ROR with increasing optimized BESS capacity in SE1 and SE2 using the scenario 2 profile. The minimum required BESS capacity to have a positive ROR for the purposes of energy shifting is 15 MWh in both areas, with an ROR of 36.9% and 37.7% for SE1 and SE2, respectively. This represents approximately a 40 % increase in ROR compared to the scenario 1 profile. Therefore, the results suggest a profit for BESS installations in SE1 and SE2 with increased adoption of renewable energy in the future.

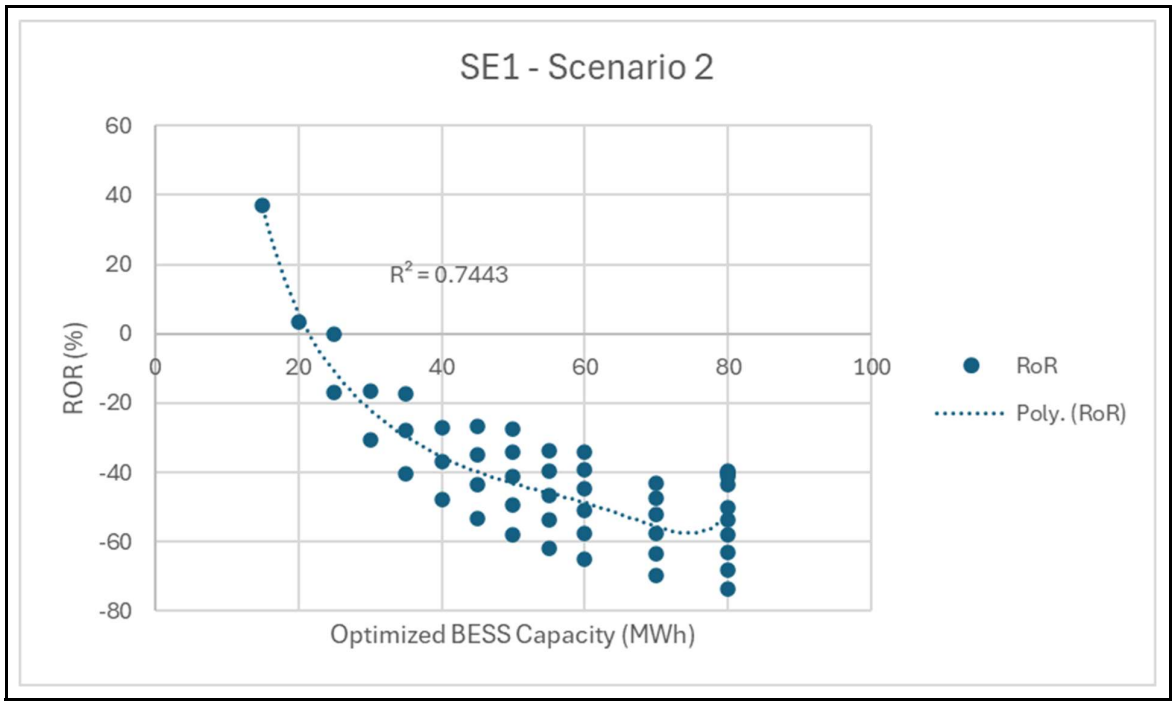

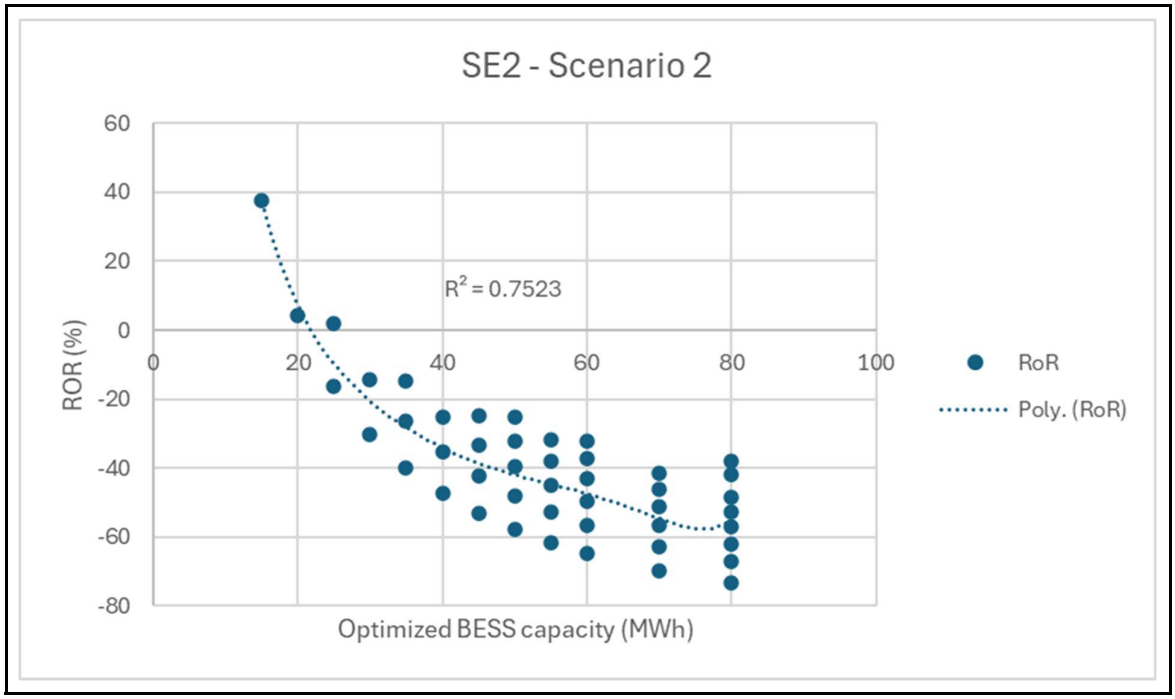

Figure 30 Scenario 2 - Comparison of ROR and optimized BESS capacity size in SE1 and SE2

In SE3 and SE4 the results are different from SE1 and SE2. In SE3 the BESS capacity of 5 MWh, 15 MWh and 25 MWh yields a gain or profit on the investment. Conversely, a BESS capacity of 5 MWh and 25 MWh is required in SE4. The results suggest an increase in ROR in scenario 2 compared to scenario 1.

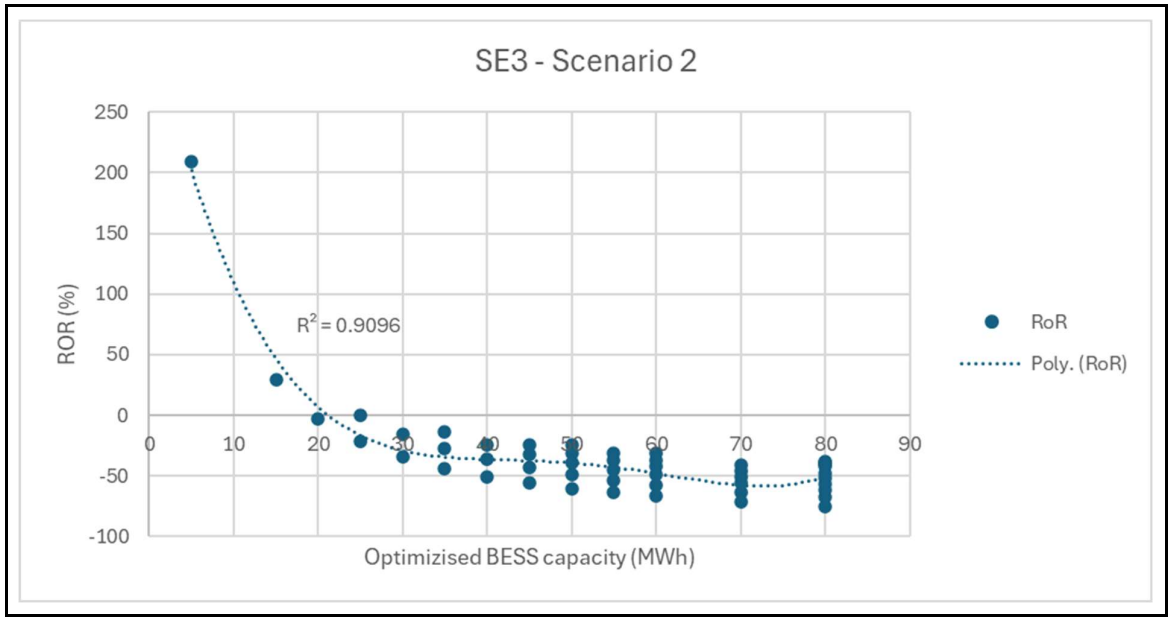

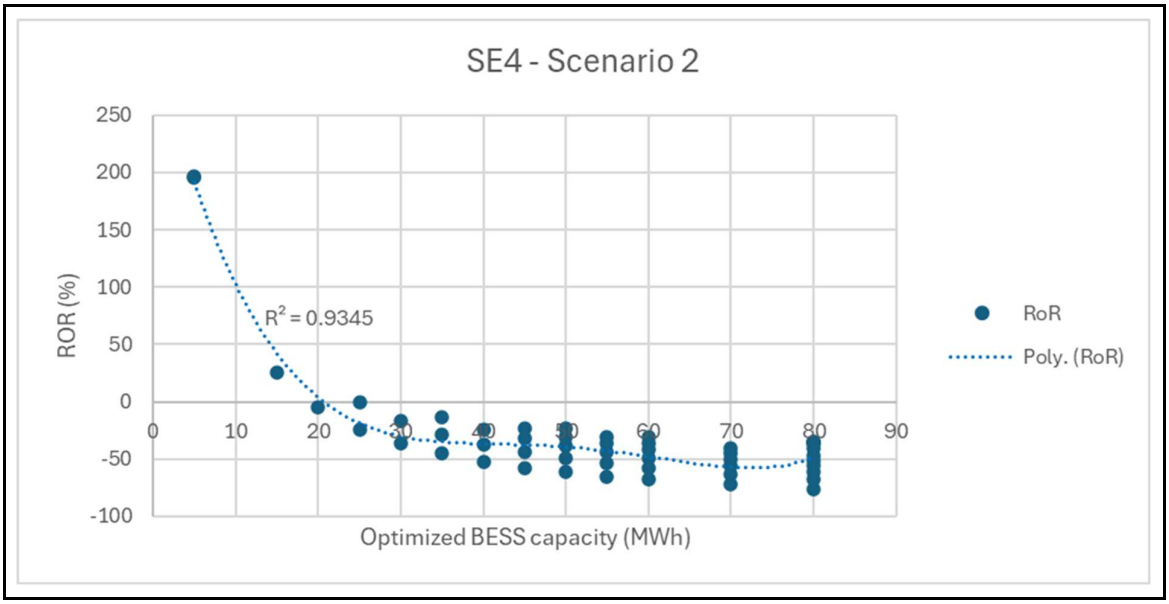

Figure 31 Scenario 2 - Comparison of ROR and optimized BESS capacity size in SE3 and SE4

Reflecting on the results, one aspect is clear, the spot price profile in the future will not be the same as those of the 2023 financial year for instance, hence investment in BESS for the purpose of energy shifting applications in SE1 and SE2 may be profitable or not in future. Furthermore, the minimum BESS capacity required for energy shifting and constant power ranges between 10MWh and 20MWh.

Table 4 Summary of minimum energy shifting capacity sizes for all price areas

Price area	**Scenario**	**C_bn (MWh)**	**P_cn (MW)**	**S2P**
SE1	Scenario 1	20	0.5	2
	Scenario 2	15	0.5	1.5
SE2	Scenario 1	20	0.5	2
	Scenario 2	15	0.5	1.5
SE3	Scenario 1	5	0.5	0.5
	Scenario 2	5	1.5	0.5
SE4	Scenario 1	20	0.5	2

	Scenario 2	5	1.5	0.5

4.3.3 BESS market size - Scenario 1

The S2P ratios shown in Table 4 were used to determine the optimized BESS capacity required to be installed on existing solar farms in Sweden based on their installed power ratings. The number of 40-foot BESS containers needed and the space requirements are also calculated. The table showing the BESS market size for solar farms with installed power greater than 1MW using Scenario 1 can be found in Appendix A. A total of 116, 40-foot BESS containers are required for the purposes of energy shifting. The total market size translates to 60 million USD.

4.4 Constant Power

As discussed in the methodology section, the main purpose of the constant power supply scenario is to analyze and optimize the proper BESS size depending on the geographical location of the solar (solar irradiation), S2P and CPO. In this scenario, the photovoltaic panels and the battery storage must at all times supply the electrical grid with constant power. During the winter season, when solar irradiation is lower than in the summer, the average power exported to the grid is smaller compared to during the summer. Figure 35 below shows the simulation results for Trelleborg in SE4 with S2P equal to 4. The figure illustrates the energy distribution over one day in summer. Observing the trend, it is evident PV power exhibits fluctuations throughout the period. The PV power starts to increase steadily from around 6 AM before reaching the peak value of approximately 7 MW at noon. It then starts to reduce and reaches 0 MW at 8 PM. This variability is expected and can be attributed to external factors such as weather conditions and time of day.

On the other hand, the grid power remains relatively constant and stable, hovering around 2.5 MW consistently. This greatly improves grid reliability- the grid's ability to provide adequate power at any time to meet projected demand, especially during disturbances that could lead to blackouts. This constant power supply to the grid is achieved by the contribution from the photovoltaic panels and BESS, as clearly illustrated by the lower figure. The BESS performance is notable, clearly demonstrating its capability to store and discharge energy effectively. In the morning when PV power is lower than grid power, the deficit is supplemented by BESS and as a result, capacity reduces towards the SOC minimum. As the day progresses, the PV power exceeds the grid power. In this case, the surplus power is used to charge BESS. This is clearly shown by the increase in capacity towards noon.

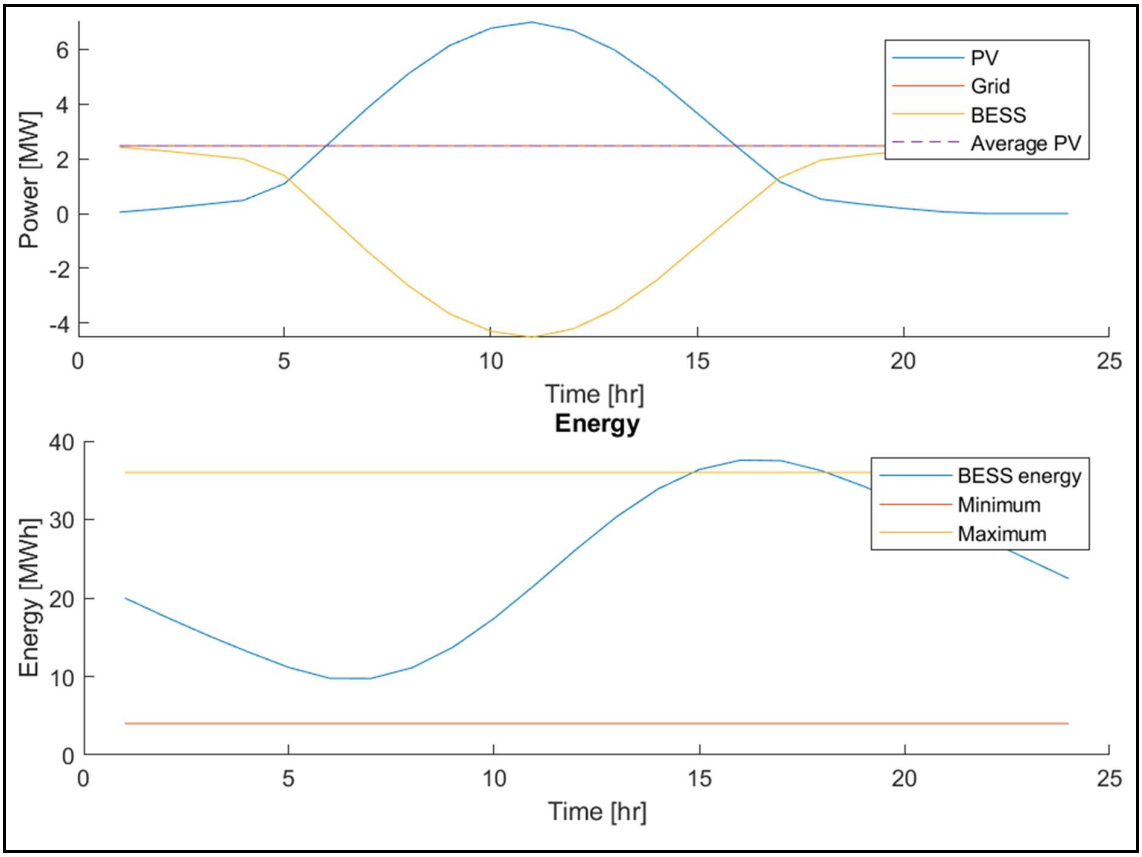

Figure 32 Constant power BESS application and SOC in SE1

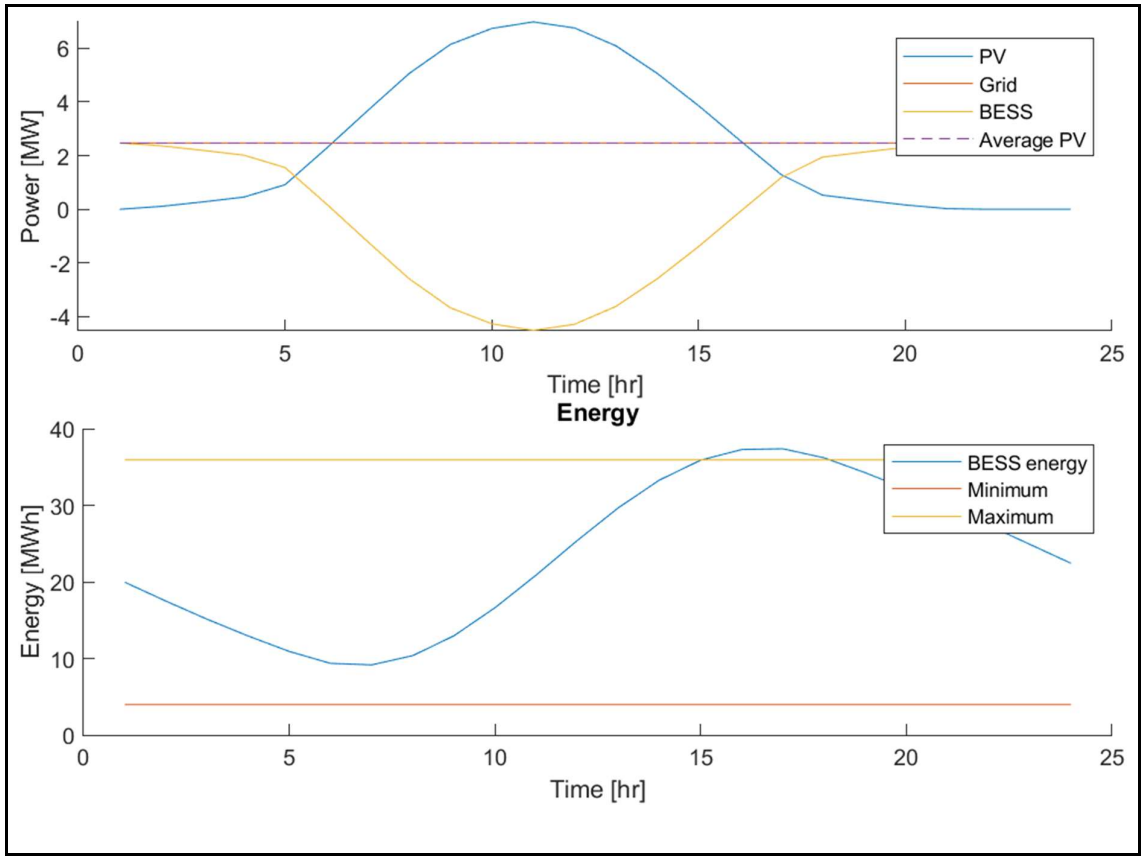

Figure 33 Constant power BESS application and SOC in SE2

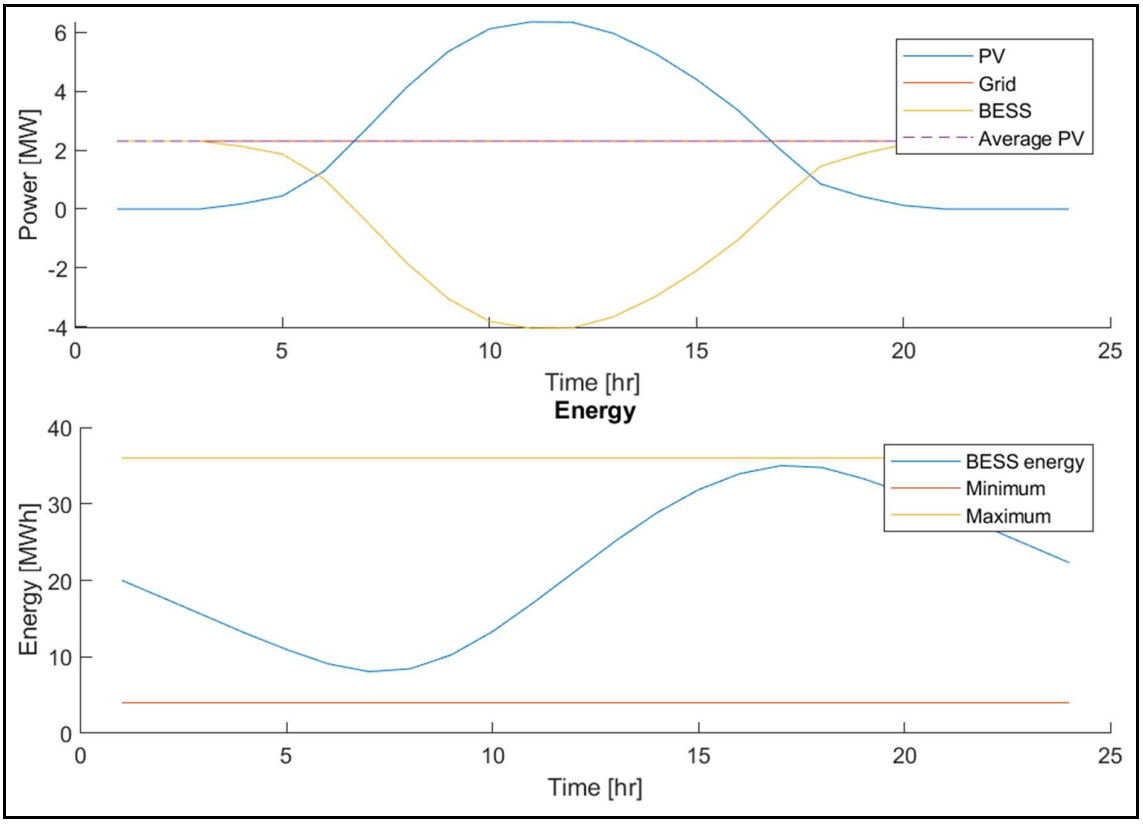

Figure 34 Constant power BESS application and SOC in SE3

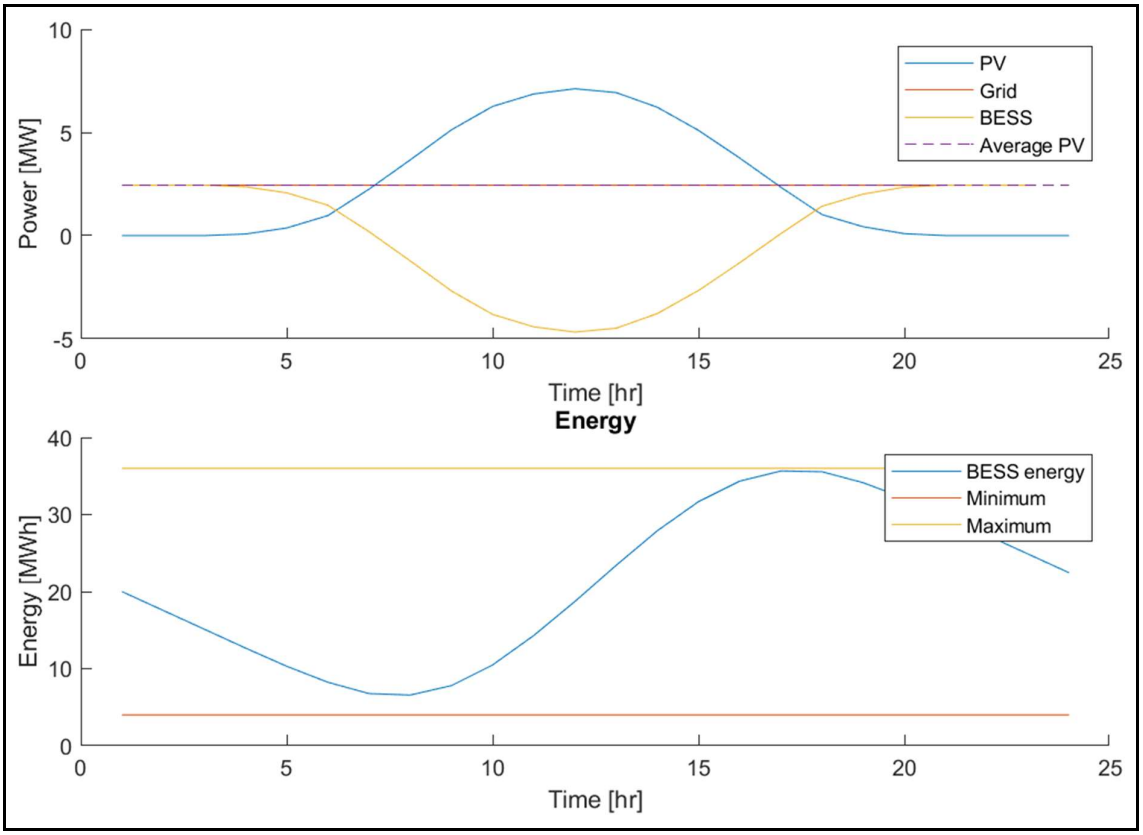

Figure 35 Constant power BESS application and SOC in SE4

It is important to note that different S2P ratios were simulated for SE1, SE2, SE3 and S4 to find the optimized BESS capacities without violating SOC and ED. The ED parameter was used as the main criterion for choosing the minimum S2P value that guaranteed no minimum and maximum SOC operating value violation. This parameter determines whether the installation meets the demanded constant power supply to the grid or not. In other words, the ED parameter is equivalent to the capacity factor of the installation. For instance, a 5 % AED (Annual Energy Deficit) parameter is equivalent to 95 % of energy availability. In Figure 32 and 33, SOC slightly exceeds the maximum SOC, however, it is possible to discharge the extra energy into, for example hydrogen production, etc.

Table 5 and Figure 36 show how different BESS capacities affect the energy deficit of the installation according to storage size (S2P) in all price areas in Sweden. The curve in Figure 35 clearly shows that the AED is inversely proportional to storage size (S2P). For lower values of S2P, AED rapidly reduces before coming to a plateau point around S2P equal to 3. After this point, an increase in the S2P only entails an increase in BESS capacity, investment cost and space requirement without any significant reduction in the AED. The selection of the suitable S2P for each price area in Sweden is based on the plateau point of the curve in Figure 35. The other important aspect considered is SOC. As stated in the literature review chapter, the lifespan of the BESS is greatly affected by SOC. In order to ensure the profitability of the BESS installation, the minimum and maximum SOC operating range is kept at 20% and 80% of BESS capacity, as shown in Figures 32 - 35.

Table 5 Summary of minimum constant power delivery capacity sizes for all price areas

S2P	**C_{bn}**	**ED**	**SP**	**Comment**
1	10	0.1138	0.2307	Violation of the minimum and maximum SOC operating range
2	20	0.0336	0.0917	Violation of the minimum and maximum SOC operating range
3	30	0	0	Violation of the maximum SOC operating range
4	40	0	0	No violation of the minimum and maximum SOC operating range
5	50	0	0	No violation of the minimum and maximum SOC operating range

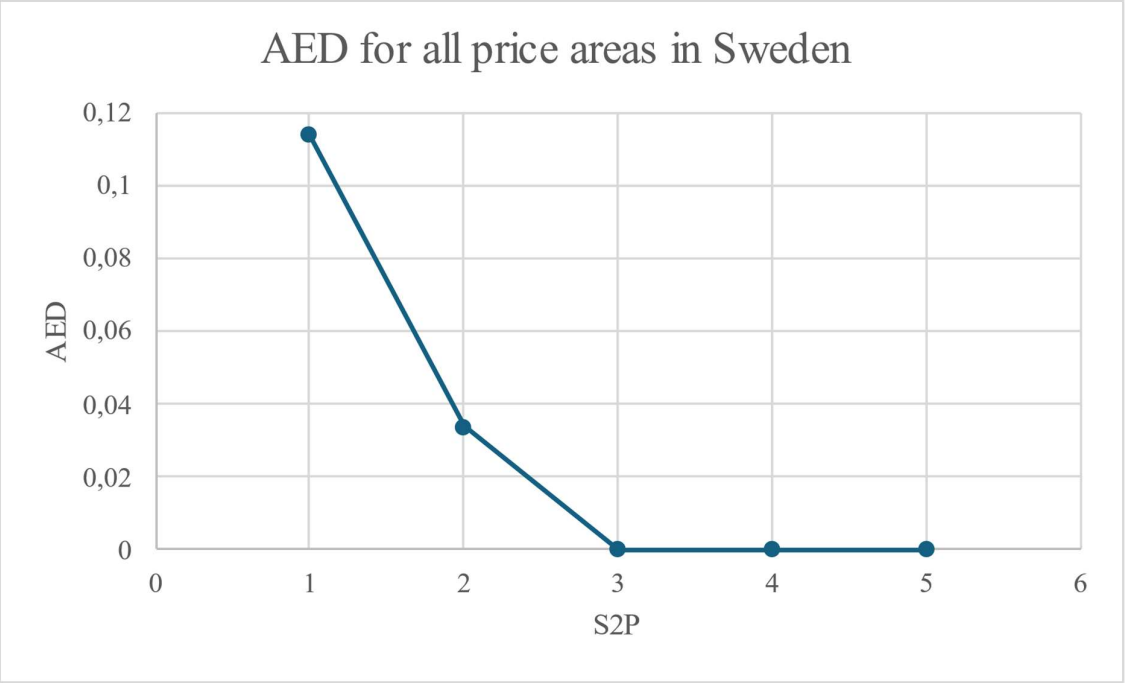

Figure 36 Annual Energy Deficit for all price areas in Sweden

4.4.1 Constant power BESS market size

Once the storage size (S2P) for each price area in Sweden was determined, it was used to determine the required BESS capacity, the number of 40-foot BESS containers, and the space needed for the BESS installation on site. Table 6 below shows the manufacturer data for the reference 40-foot BESS container that was used in the calculation (Energy storage container, BESS container, 2024).

Table 6 Manufacturer data for 40-foot BESS container (Energy storage container, BESS container, 2024)

Model		**ZESS2580K**
Parameters	Rated Capacity	2.58MWH
	Configuration	12 Sets 768V280AH BESS
	Voltage	768V
	Working voltage rage	DC672V ~ DC876V （2.8V ~ 3.65V）
	Battery type	LFP
	Dimensions	12196*2438*2591mm

Figure 37 Reference BESS Container ('Energy storage container, BESS container', 2024)

The analysis of 40ft Battery Energy Storage Systems (BESS) deployment across various solar parks in Sweden reveals a diverse landscape marked by capacity and spatial requirements variation. Examining smaller installations, such as Brf. Opalen and Beslag & Merall in SE4 and SE3, respectively in Appendix B, require 2 40-foot BESS container units each, with a BESS capacity of 4 MWh of energy and occupying 60 square meters. On the other end of the spectrum, larger installations like Kungsåra Solpark and Strängnäs Solcellspark demonstrate considerable capacities, housing 35 and 30 BESS container units, with capacities of 88 and 84 MWh of energy, respectively. These installations span significant areas, with Kungsåra Solpark covering 1040 square meters and Strängnäs Solcellspark occupying 980 square meters in SE3.

Moreover, the spatial requirements and costs associated with these installations vary significantly across regions. For instance, installations situated in SE3 demand more space and incur higher costs than those in SE4. This trend is exemplified by installations like Hallstahammar and Vimmerby, which require 446 square meters and 1040 square meters, respectively, in SE3. Conversely, SE4 locations like Hörby and Hultsfred accommodate smaller footprints and entail lower expenses, with Hörby in SE4 covering 852 square meters.

The findings underscore the pivotal role of localized factors in shaping the deployment strategies of solar parks and associated BESS infrastructure. This emphasizes the need for flexible and context-sensitive approaches in renewable energy planning. By tailoring investments to align with specific regional requirements, resource utilization can be optimized, and the economic viability of renewable energy projects can be enhanced. Furthermore, the observed variations highlight the need for flexible and context-sensitive approaches in renewable energy planning to ensure resilience and sustainability amidst evolving energy landscapes.

Looking ahead, the potential of integrating technological advancements and leveraging data-driven insights in refining decision-making processes in solar park development is significant. By harnessing predictive analytics and scenario modelling, stakeholders can anticipate future energy demands and optimize BESS configurations to maximize efficiency and cost-effectiveness. Additionally, fostering collaboration among policymakers, industry

stakeholders, and research institutions can facilitate knowledge exchange and drive innovation in renewable energy deployment strategies.

4.4.2 BESS market size - Scenario 2

The S2P ratios of 4 shown in Table 4 were chosen to determine the optimized BESS capacity required to be installed on existing solar farms in Sweden based on their installed power ratings. The number of 40-foot BESS containers needed and the space requirements are also calculated. The table showing the BESS market size for solar farms with installed power greater than 1MW using Scenario 2 can be found in Appendix B. A total of 397, 40-foot BESS containers are required for the purposes of constant power. The total market size translates to 243,840,000 USD.

Figure 38 below summarizes the space requirement for an 18 MW solar farm in Skurup. The yellow color shows the PV panel area, red represents the energy shifting BESS space, and blue indicates the space required for constant power BESS. The figure clearly shows a smaller area requirement for BESS installation compared to the area needed to install PV panels.

Figure 38 Space requirement for 18MW Skurup solar farm with BESS installation, red square: BESS installation for energy shifting, blue square: BESS installation for constant power, yellow area: solar farm (MyMaps, Google)

Conclusion

In this work, two main methods for optimal BESS size analysis were applied - energy shifting and constant power. Energy shifting service allows investors to increase their profit by selling the produced energy during high demand. This possibility may result in the overall profitability of the system and could help the deployment of BESS at a higher rate.

For energy shifting, it was found that the optimum size ratio for price scenario 1 is 2 MWh/MW for SE1, SE2, and SE4. For the SE3 region, the optimum ratio was found to be 0.5, 1, and 1.5 MWh/MW. Borkowski et al. (2023) found the optimum size ratio to be 2 MWh/MW which corresponds to the findings of this work, with an exception for SE3. The simulation showed positive ROR for both SE3 and SE4. However, for SE1 and SE2, the overall ROR was negative, suggesting that the solar irradiation, and spot prices in the northern regions do not create suitable conditions for the deployment of the system. It should be noted that in the future, the expected decrease in system prices might result in its profitability. Also, the utilized model was limited to solely selling the produced energy from the solar farm at the most profitable time. The calculations did not include buying energy from the grid. The market size for energy shifting service analysis suggests the possibility of deploying 116 BESS containers with a total capacity of 230 MWh. This market size analysis includes all solar parks in Sweden above 1 MW (also applicable for constant power delivery market size).

Price scenario 2 (high solar penetration) for energy shifting significantly improved ROR and affected optimum size ratios. For S1 and SE2, the optimum was 1.5 MWh with positive ROR that increased by 40 % compared to the price scenario 1. For SE3, the optimum ratios turned out to be 0.5, 1.5, and 2.5 MWh/MW with positive ROR. In the case of SE4, the optimum ratios were found to be 0.5 and 2.5 MWh/MW with positive ROR. Compared to price scenario 1, all price areas increased their profitability for BESS installment and thus suggest their possible attractiveness in the future.

The second studied service - constant power delivery was evaluated from the power firmness (secure and predictable power) perspective using the energy deficit indicator. The results show that for all price areas, the optimum size ratio was (S2P) 4. This ratio yields no energy deficit or surplus. Furthermore, the market size analysis shows that if all solar farms in Sweden utilized BESS for constant power delivery, it would require 397 BESS containers with a total capacity of 975 MWh.

In conclusion, the optimum S2P ratio for energy shifting was found to be 2 MWh/MW with an exception for SE3. The system was profitable for southern regions (SE3, SE4), but the ROR was negative for SE1 and SE2. However, in the future with the increased solar energy penetration, the BESS could generate positive revenue for investors even in the northern regions. As for the constant power, the ideal S2P ratio was 4 MWh/MW for all regions in Sweden. For future research, as the optimum size ratios differ significantly for the two

studied services, it highlights the importance of understanding the size requirements for the numerous services the BESS can provide.

References

6.5. Efficiency of Inverters | EME 812: Utility Solar Power and Concentration (no date). Available at: https://www.e-education.psu.edu/eme812/node/738 (Accessed: 14 April 2024).

A Guide to Solar Panel Sizes, Dimensions & Wattages in The UK (no date) *GreenMatch.co.uk*. Available at: https://www.greenmatch.co.uk/solar-energy/solar-panels/sizes (Accessed: 27 May 2024).

Anläggningar över 1 MW (no date) *Svensk Solenergi*. Available at: https://svensksolenergi.se/om-solenergi/anlaggningar/solcellsparker/ (Accessed: 27 May 2024).

Badeda, J. *et al.* (2017) 'Adaptive battery steering and management system for the optimized operation of stationary battery energy storage systems in multi-use applications', in *2017 IEEE International Telecommunications Energy Conference (INTELEC)*. *2017 IEEE International Telecommunications Energy Conference (INTELEC)*, Broadbeach, QLD: IEEE, pp. 287–293. Available at: https://doi.org/10.1109/INTLEC.2017.8214149.

Bank, A.D. (2018) *Handbook on Battery Energy Storage System*. Asian Development Bank. Available at: https://www.adb.org/publications/battery-energy-storage-system-handbook (Accessed: 10 April 2024).

Bayod-Rújula, Á.A., Haro-Larrodé, M.E. and Martínez-Gracia, A. (2013) 'Sizing criteria of hybrid photovoltaic–wind systems with battery storage and self-consumption considering interaction with the grid', *Solar Energy*, 98, pp. 582–591. Available at: https://doi.org/10.1016/j.solener.2013.10.023.

Borkowski, D., Oramus, P. and Brzezinka, M. (2023) 'Battery energy storage system for grid-connected photovoltaic farm – Energy management strategy and sizing optimization algorithm', *Journal of Energy Storage*, 72, p. 108201. Available at: https://doi.org/10.1016/j.est.2023.108201.

Braga, D. (2023) 'Power Quality Considering the Massive Integration of Variable Renewable Energy Sources: 2023 International Conference on Electromechanical and Energy Systems (SIELMEN), Electromechanical and Energy Systems (SIELMEN), 2023 International Conference on', *2023 International Conference on Electromechanical and Energy Systems (SIELMEN), Electromechanical and Energy Systems (SIELMEN), 2023 International Conference on*, pp. 1–6. Available at: https://doi.org/10.1109/SIELMEN59038.2023.10290824.

Cao, J. *et al.* (2020) 'Deep Reinforcement Learning-Based Energy Storage Arbitrage With Accurate Lithium-Ion Battery Degradation Model', *IEEE Transactions on Smart Grid*, 11(5), pp. 4513–4521. Available at: https://doi.org/10.1109/TSG.2020.2986333.

Cole, W., Frazier, A.W. and Augustine, C. (2021) 'Cost Projections for Utility-Scale Battery Storage: 2021 Update', *Renewable Energy* [Preprint].

Commission Regulation (EU) 2016/631 of 14 April 2016 establishing a network code on requirements for grid connection of generators (Text with EEA relevance) (2016) *OJ L*. Available at: http://data.europa.eu/eli/reg/2016/631/oj/eng (Accessed: 9 April 2024).

Das, C.K. *et al.* (2018) 'Overview of energy storage systems in distribution networks: Placement, sizing, operation, and power quality', *Renewable and Sustainable Energy Reviews*, 91, pp. 1205–1230. Available at: https://doi.org/10.1016/j.rser.2018.03.068.

Datta, U., Kalam, A. and Shi, J. (2021) 'A review of key functionalities of battery energy storage system in renewable energy integrated power systems', *Energy Storage*, 3(5). Available at: https://doi.org/10.1002/est2.224.

Do, P. *et al.* (2022) 'Understanding the Impact of Spot Market Electricity Price on Wastewater Asset Management Strategy', *Water Conservation Science and Engineering*, 7(2), pp. 101–117. Available at: https://doi.org/10.1007/s41101-022-00132-5.

Dustmann, C.-H. and Bito, A. (2009) *Secondary Batteries – High Temperature Systems: Safety*. Elsevier, Inc (Encyclopedia of Electrochemical Power Sources), p. 333.

EEA (2024) *Share of energy consumption from renewable sources in Europe*. Available at: https://www.eea.europa.eu/en/analysis/indicators/share-of-energy-consumption-from (Accessed: 15 May 2024).

Energinet (no date) *Home*, *Energinet*. Available at: https://www.energidataservice.dk/tso-electricity/NordpoolMarket (Accessed: 14 April 2024).

'Energy storage container, BESS container' (2024) *https://www.scupower.com/*. Available at: https://www.scupower.com/energy-storage/energy-storage-container/ (Accessed: 21 May 2024).

Feder, D.O., Hlavac, M.J. and Koster, W. (1993) 'Evaluating the state-of-health of flooded and valve-regulated lead/acid batteries. A comparison of conductance testing with traditional methods', in 01/01/1994 (ed.). *Journal of Power Sources*, Varna, Switzerland, Bulgaria, pp. 391–415.

Garside (2022) *U.S. nuclear power plants' capacity factor 2022*, *Statista*. Available at: https://www.statista.com/statistics/191201/capacity-factor-of-nuclear-power-plants-in-the-us-since-1975/ (Accessed: 15 May 2024).

Hannan, M.A. *et al.* (2021) 'Battery energy-storage system: A review of technologies, optimization objectives, constraints, approaches, and outstanding issues', *Journal of Energy Storage*, 42, p. 103023. Available at: https://doi.org/10.1016/j.est.2021.103023.

How does the electricity market work? (no date). Available at: http://www.tekniskaverken.se/privat/other-languages/save-electricity/electricity-market/ (Accessed: 14 April 2024).

Information regarding network codes for grid connection (2020). Available at: https://ei.se/ei-in-english/electricity/information-regarding-network-codes-for-grid-connection (Accessed: 9 April 2024).

Ingman, T. and Sivers, H.V. (2023) 'Unlocking the Potential of Battery Energy Storage Systems in the Nordic Frequency Regulation Markets'.

IRENA (2017) 'Electricity storage and renewables: Costs and markets to 2030'.

IRENA (2019) *Global energy transformation: A roadmap to 2050 (2019 edition)*. Available at: https://www.irena.org/publications/2019/Apr/Global-energy-transformation-A-roadmap-to-2050-2019Edition (Accessed: 15 May 2024).

Jinlei, S. *et al.* (2019) 'Economic Operation Optimization for 2nd Use Batteries in Battery Energy Storage Systems', *IEEE Access*, 7, pp. 41852–41859. Available at: https://doi.org/10.1109/ACCESS.2019.2902402.

JRC Photovoltaic Geographical Information System (PVGIS) - European Commission (no date). Available at: https://re.jrc.ec.europa.eu/pvg_tools/en/tools.html (Accessed: 14 April 2024).

Juhlin, O. (2016) 'Modeling of Battery Degradation in Electrified Vehicles'.

Khalilisenobari, R. and Wu, M. (2021) 'Impact of Battery Degradation on Market Participation of Utility-Scale Batteries: Case Studies', in *2020 52nd North American Power Symposium (NAPS)*. *2020 52nd North American Power Symposium (NAPS)*, pp. 1–6. Available at: https://doi.org/10.1109/NAPS50074.2021.9449728.

Koleti, U.R., Dinh, T.Q. and Marco, J. (2020) 'A new on-line method for lithium plating detection in lithium-ion batteries', *Journal of Power Sources*, 451, p. 227798. Available at: https://doi.org/10.1016/j.jpowsour.2020.227798.

Lag om ändring i ellagen (1997:857) | Svensk författningssamling (no date). Available at: https://svenskforfattningssamling.se/doc/2022596.html (Accessed: 9 April 2024).

Liu, C., Gao, Y. and Liu, L. (2021) 'Toward safe and rapid battery charging: Design optimal fast charging strategies thorough a physics-based model considering lithium plating', *International Journal of Energy Research*, 45(2), pp. 2303–2320. Available at: https://doi.org/10.1002/er.5924.

López Prol, J., Steininger, K.W. and Zilberman, D. (2020) 'The cannibalization effect of wind and solar in the California wholesale electricity market', *Energy Economics*, 85, p. 104552. Available at: https://doi.org/10.1016/j.eneco.2019.104552.

Mehar, D., Singh, R.K. and Gupta, A.K. (2023a) 'A Review on Battery Technologies and Its Challenges in Electrical Vehicle', in *2023 IEEE International Students' Conference on Electrical, Electronics and Computer Science (SCEECS)*. *2023 IEEE International Students' Conference on Electrical, Electronics and Computer Science (SCEECS)*, pp. 1–6. Available at: https://doi.org/10.1109/SCEECS57921.2023.10063067.

Mehar, D., Singh, R.K. and Gupta, A.K. (2023b) 'A Review on Battery Technologies and Its Challenges in Electrical Vehicle', in *2023 IEEE International Students' Conference on Electrical, Electronics and Computer Science (SCEECS)*. *2023 IEEE International Students' Conference on Electrical, Electronics and Computer Science (SCEECS)*, Bhopal, India: IEEE, pp. 1–6. Available at: https://doi.org/10.1109/SCEECS57921.2023.10063067.

Mongird, K. *et al.* (2020) '2020 Grid Energy Storage Technology Cost and Performance Assessment'.

Muqbel, A. *et al.* (2018) 'Fuzzy Optimization-based Sizing of a Battery Energy Storage System for Participating in Ancillary Services Markets', in, pp. 1–7. Available at: https://doi.org/10.1109/IAS.2018.8544661.

Naumann, M. *et al.* (2018) 'Analysis and modeling of calendar aging of a commercial LiFePO4/graphite cell', *Journal of Energy Storage*, 17, pp. 153–169. Available at: https://doi.org/10.1016/j.est.2018.01.019.

Nord Pool | Day-ahead prices (no date). Available at: https://data.nordpoolgroup.com/auction/day-ahead/prices?deliveryDate=2024-05-

24&currency=EUR&aggregation=Hourly&deliveryAreas=SE1,SE2,SE3,SE4 (Accessed: 27 May 2024).

Open Infrastructure Map (no date). Available at: https://openinframap.org/stats/area/Sweden/plants (Accessed: 27 May 2024).

Photovoltaic Energy Factsheet (no date) *Center for Sustainable Systems*. Available at: https://css.umich.edu/publications/factsheets/energy/photovoltaic-energy-factsheet (Accessed: 14 April 2024).

Pi, X. and Liu, Q. (2024) 'Analysis of the relationship between operating parameters and health state of power batteries', in *Ninth International Conference on Energy Materials and Electrical Engineering (ICEMEE 2023)*. *Ninth International Conference on Energy Materials and Electrical Engineering (ICEMEE 2023)*, SPIE, pp. 1308–1312. Available at: https://doi.org/10.1117/12.3015327.

Raijmakers, L.H.J. *et al.* (2019) 'A review on various temperature-indication methods for Li-ion batteries', *Applied Energy*, 240, pp. 918–945. Available at: https://doi.org/10.1016/j.apenergy.2019.02.078.

Rakhimov, E. *et al.* (2024) 'Battery technologies: exploring different types of batteries for energy storage', *BIO Web of Conferences*. Edited by M.-T. Liong and I.V. Tkacheva, 84, p. 05034. Available at: https://doi.org/10.1051/bioconf/20248405034.

Recommendations on energy storage (no date). Available at: https://energy.ec.europa.eu/topics/research-and-technology/energy-storage/recommendations-energy-storage_en (Accessed: 4 April 2024).

Renewables - Energy System (no date) *IEA*. Available at: https://www.iea.org/energy-system/renewables (Accessed: 5 April 2024).

Richard, B., Pivert, X. and Bourien, Y.-M. (2020) *BESS Optimal Sizing Methodology - Degree of Impact of Several Influencing Factors*.

Saâdaoui, F. and Ben Jabeur, S. (2023) 'Analyzing the influence of geopolitical risks on European power prices using a multiresolution causal neural network', *Energy Economics*, 124, p. 106793. Available at: https://doi.org/10.1016/j.eneco.2023.106793.

Sandelic, M., Sangwongwanich, A. and Blaabjerg, F. (2022) 'Incremental Degradation Estimation Method for Online Assessment of Battery Operation Cost', *IEEE Transactions on Power Electronics*, 37(10), pp. 11497–11501. Available at: https://doi.org/10.1109/TPEL.2022.3172499.

Sandhya Lavety; Ritesh Kumar Keshri; Madhuri A. Chaudhari (2020) *Evaluation of Charging Strategies for Valve Regulated Lead-Acid Battery | IEEE Journals & Magazine | IEEE Xplore*. Available at: https://ieeexplore.ieee.org/document/9187255 (Accessed: 13 April 2024).

Setting the power price: the merit order effect (2015) *Clean Energy Wire*. Available at: https://www.cleanenergywire.org/factsheets/setting-power-price-merit-order-effect (Accessed: 15 May 2024).

Shi, Y. *et al.* (2018) 'A Convex Cycle-based Degradation Model for Battery Energy Storage Planning and Operation', in *2018 Annual American Control Conference (ACC)*. *2018 Annual American Control Conference (ACC)*, pp. 4590–4596. Available at: https://doi.org/10.23919/ACC.2018.8431814.

SMHI (2024) *Normal global radiation during a year | SMHI*. Available at: https://www.smhi.se/data/meteorologi/stralning/normal-globalstralning-under-ett-ar-1.2927 (Accessed: 22 May 2024).

Solcellspark (no date) *Göteborg Energi*. Available at: https://www.goteborgenergi.se/foretag/solceller/solcellspark (Accessed: 14 April 2024).

Spot Market Prices | Energy-Charts (no date). Available at: https://energy-charts.info/charts/price_spot_market/chart.htm?l=en&c=SE&interval=year&year=2023 (Accessed: 26 May 2024).

Swami, R. and Gupta, S.K. (2022) 'Optimization of Standalone Microgrid's Operation Considering Battery Degradation Cost', in R.C. Bansal et al. (eds) *Proceedings of International Conference on Computational Intelligence and Emerging Power System*. Singapore: Springer, pp. 267–277. Available at: https://doi.org/10.1007/978-981-16-4103-9_23.

Tejero-Gómez, J.A. (2023) 'Analysis of Photovoltaic Plants with Battery Energy Storage Systems (PV-BESS) for Monthly Constant Power Operation', *Energies*, 16(13), p. 4909. Available at: https://doi.org/10.3390/en16134909.

Trilochana, S. and Sangeetha, C.N. (2021) 'A Comparative study and Recent Research of Battery Technologies', (0886).

United, N. (no date) *Renewable energy – powering a safer future*, *United Nations*. United Nations. Available at: https://www.un.org/en/climatechange/raising-ambition/renewable-energy (Accessed: 4 April 2024).

USD to EUR Exchange Rate (no date) *Bloomberg.com*. Available at: https://www.bloomberg.com/quote/USDEUR:CUR (Accessed: 9 May 2024).

What is spot price (spotpris)? (no date). Available at: http://www.tekniskaverken.se/privat/other-languages/save-electricity/spot-price/ (Accessed: 20 May 2024).

'Wholesale Price - Definition, Wholesale vs. Retail Price' (2023), 17 January. Available at: https://www.sniffie.io/pricing-vocabulary/wholesale-price/ (Accessed: 27 May 2024).

Xie, W. and Yang, S. (2023) 'Charging Optimization of Lithium-Ion Batteries Based on Charge Transfer Limitation and Mass Transport Limitation', *Journal of The Electrochemical Society*, 170(1), p. 010506. Available at: https://doi.org/10.1149/1945-7111/acaf3d.

Xu, B., Zhao, J., *et al.* (2018) 'Factoring the Cycle Aging Cost of Batteries Participating in Electricity Markets', in *2018 IEEE Power & Energy Society General Meeting (PESGM)*. *2018 IEEE Power & Energy Society General Meeting (PESGM)*, pp. 1–1. Available at: https://doi.org/10.1109/PESGM.2018.8586232.

Xu, B., Oudalov, A., *et al.* (2018) 'Modeling of Lithium-Ion Battery Degradation for Cell Life Assessment', *IEEE Transactions on Smart Grid*, 9(2), pp. 1131–1140. Available at: https://doi.org/10.1109/TSG.2016.2578950.

Yan, J. *et al.* (2011) 'Model Predictive Control-Based Fast Charging for Vehicular Batteries', *Energies*, 4(8), pp. 1178–1196. Available at: https://doi.org/10.3390/en4081178.

Yang, Y. *et al.* (2018) 'Battery energy storage system size determination in renewable energy systems: A review', *Renewable and Sustainable Energy Reviews*, 91, pp. 109–125. Available at: https://doi.org/10.1016/j.rser.2018.03.047.

Yao, G. *et al.* (2022) 'Adaptive Grid Partitioning Considering Power Supply and Load Distribution', *IEEE Access*, 10, pp. 111066–111076. Available at: https://doi.org/10.1109/ACCESS.2022.3208886.

Yoo, Y., Jang, G. and Jung, S. (2022) 'Stochastic assessment of frequency support from wind power plants for power system with high wind penetration using correlation between wind farms', *IET Renewable Power Generation*, 16(11), pp. 2372–2383. Available at: https://doi.org/10.1049/rpg2.12528.

(No date). Available at: https://www.irena.org/publications/2019/Apr/Global-energy-transformation-A-roadmap-to-2050-2019Edition (Accessed: 3 June 2024).

5 Appendix A: BESS market size – Energy Shifting

Solar park	Power rating [MW]	S2P [hours]	Cbn [MWh]	No. of 40ft BESS container	Space needed [m2]	Price areas	Location
Åbro bryggeri solpark	7.5	0.5	**3.75**	**2**	59.4677	SE3	Vimmerby
Solcellsparken I Hallstahammar	9.5	0.5	**4.75**	**2**	59.4677	SE3	Hallstahammar
Kungsåra Solcellspark	22	0.5	**11**	**5**	148.669	SE3	Kungsåra
Fjällskär	20.2	0.5	**10.1**	**4**	118.935	SE3	Fjällskär
Hörby	18	2	**36**	**14**	416.274	SE4	Hörby
Hultsfred solcellspark	2.5	2	**5**	**2**	59.4677	SE4	Hulstsfred
Notalo Solpark	7.5	2	**15**	**6**	178.403	SE4	Åhus
Martin & Serveras solpark	18	2	**36**	**14**	416.2739	SE4	Skurup
Solparken I Forsby	3	2	**6**	**3**	89.2015	SE4	Klippan
MP bolagen Industri AB	1.15	0.5	**0.575**	**1**	29.7339	SE3	Vetlanda
Brf. Opalen	1.05	0.5	**0.525**	**1**	29.7339	SE4	Norrköping
Sparbanken Skånes Solcellspark	18	0.5	**9**	**4**	118.935	SE3	Sjöbo
Solinavium	5.5	0.5	**2.75**	**2**	59.4677	SE3	Utby
Varberg Norra	4.8	0.5	**2.4**	**1**	29.7339	SE3	Varberg
Fyrislund	4.4	0.5	**2.2**	**1**	29.7339	SE3	Uppsala
Komatsu Umeå	3.2	2	**6.4**	**3**	89.2015	SE1	Umeå
Solcellspark Östersund	3	2	**6**	**3**	89.2015	SE2	Östersund
Solcellsparken NÄL	1.632	0.5	**0.816**	**1**	29.7339	SE3	Trollhättan
Susegården Solpark	1.517	0.5	**0.7585**	**1**	29.7339	SE3	Getinge/Kvibille
Flygstaden	1.5	0.5	**0.75**	**1**	29.73385	SE3	Eslöv
Kingspan	1.3	0.5	**0.65**	**1**	29.73385	SE3	Stigamo

SVEF Solcellspark	1.2	0.5	**0.6**	**1**	29.73385	SE3	Frillesås
Carlfors Bruk Solcellspark	1.2	0.5	**0.6**	**1**	29.73385	SE3	Huskvarna
Claro Energy Solcellspark	1.2	0.5	**0.6**	**1**	29.73385	SE3	Kungsbacka
Tågarp Flygplats Solcellspark	1.2	2	**2.4**	**1**	29.73385	SE4	Trelleborg
Beslag & Merall	1.091	0.5	**0.5455**	**1**	29.73385	SE3	Vetlanda
Strängnäs Solcellspark	21	0.5	**10.5**	**5**	148.6692	SE3	Strängnäs
Eken	12	0.5	**6**	**3**	89.20154	SE3	Linköping
Solskenet	5	0.5	**2.5**	**1**	29.73385	SE3	Borås
Solpunkten C4 Energi	4	2	**8**	**4**	118.9354	SE4	Kristianstad
Hisingen Logistikpark	3.7	0.5	**1.85**	**1**	29.73385	SE3	Göteborg
Elvireborgs Solpark	1.6	2	**3.2**	**2**	59.4677	SE4	Södra Möinge
Karlskrona Solpark	2.4	2	**4.8**	**2**	59.4677	SE4	Karlskrona
Törneby Solpark	2.25	2	**4.5**	**2**	59.4677	SE4	Kalmar
HSB BRF Bosvedjan	1.3	0.5	**0.65**	**1**	29.73385	SE3	Sundsvall
Projekt Sol 3 GWh Region Jönköping Norr	1.25	0.5	**0.625**	**1**	29.73385	SE3	Jönköping
Solpark Skas Skövde	1.2	0.5	**0.6**	**1**	29.73385	SE3	Skövde
Nya Solevi	5.5	0.5	**2.75**	**2**	59.4677	SE3	Göteborg
ETC Solpark	4	0.5	**2**	**1**	29.73385	SE3	Katrineholm
Solcellsparken I Landskrona	2.2	2	**4.4**	**2**	59.4677	SE4	Landskrona
Apotea	1.5	0.5	**0.75**	**1**	29.73385	SE3	Morgongåva
Lindbäcks	1.1	2	**2.2**	**1**	29.73385	SE2	Piteå
Solsidan	2.7	2	**5.4**	**3**	89.20154	SE4	Tvååker

Solcellsparken I Kjula	1.1	0.5	**0.55**	**1**	29.73385	SE3	Eskiltuna
Väla Centrum	1.1	2	**2.2**	**1**	29.73385	SE4	Helsingborg
Mega-Sol	1.1	0.5	**0.55**	**1**	29.73385	SE3	Arvika
Solparken	1.1	0.5	**0.55**	**1**	29.73385	SE3	Västerås
Vasakronan solcellspark	4.4	0.5	**2.2**	**1**	29.73385	SE3	Uppsala
Bredstorp Solpark	1.2	0.5	**0.6**	**1**	29.73385	SE3	Bredstorp
BESS Market Size - Scenario 1							
Cbn [MWh]	**232**						
No. of 40-foot BESS containers	**116**						
Total cost [USD]	**58 136 250**						

6 Appendix B: BESS market size – Constant Power

Solar park	Power rating [MW]	S2P [hours]	Cbn [MWh]	No. of 40ft BESS container	Space requirement	Price areas	Location
Åbro bryggeri solpark	7.5	4	**30**	**12**	356.8062	SE3	Vimmerby
Solcellsparken I Hallstahammar	9.5	4	**38**	**15**	446.0077	SE3	Hallstahammar
Kungsåra Solcellspark	22	4	**88**	**35**	1040.685	SE3	Kungsåra
Fjällskär	20.2	4	**80.8**	**32**	951.4831	SE3	Fjällskär
Hörby	18	4	**72**	**28**	832.5477	SE4	Hörby
Hultsfred solcellspark	2.5	4	**10**	**4**	118.9354	SE4	Hulstsfred
Notalo Solpark	7.5	4	**30**	**12**	356.8062	SE4	Åhus
Martin & Serveras solpark	18	4	**72**	**28**	832.5477	SE4	Skurup
Solparken I Forsby	3	4	**12**	**5**	148.6692	SE4	Klippan
MP bolagen Industri AB	1.15	4	**4.6**	**2**	59.4677	SE3	Vetlanda
Brf. Opalen	1.05	4	**4.2**	**2**	59.4677	SE4	Norrköping
Sparbanken Skånes Solcellspark	18	4	**72**	**28**	832.5477	SE3	Sjöbo
Solinavium	5.5	4	**22**	**9**	267.6046	SE3	Utby
Varberg Norra	4.8	4	**19.2**	**8**	237.8708	SE3	Varberg
Fyrislund	4.4	4	**17.6**	**7**	208.1369	SE3	Uppsala
Komatsu Umeå	3.2	4	**12.8**	**5**	148.6692	SE1	Umeå
Solcellspark Östersund	3	4	**12**	**5**	148.6692	SE2	Östersund
Solcellsparken NÄL	1.632	4	**6.528**	**3**	89.20154	SE3	Trollhättan
Susegården Solpark	1.517	4	**6.068**	**3**	89.20154	SE3	Getinge/Kvibille
Flygstaden	1.5	4	**6**	**3**	89.20154	SE3	Eslöv
Kingspan	1.3	4	**5.2**	**3**	89.20154	SE3	Stigamo

SVEF Solcellspark	1.2	4	**4.8**	**2**	59.4677	SE3	Frillesås
Carlfors Bruk Solcellspark	1.2	4	**4.8**	**2**	59.4677	SE3	Huskvarna
Claro Energy Solcellspark	1.2	4	**4.8**	**2**	59.4677	SE3	Kungsbacka
Tågarp Flygplats Solcellspark	1.2	4	**4.8**	**2**	59.4677	SE4	Trelleborg
Beslag & Merall	1.091	4	**4.364**	**2**	59.4677	SE3	Vetlanda
Strängnäs Solcellspark	21	4	**84**	**33**	981.217	SE3	Strängnäs
Eken	12	4	**48**	**19**	564.9431	SE3	Linköping
Solskenet	5	4	**20**	**8**	237.8708	SE3	Borås
Solpunkten C4 Energi	4	4	**16**	**7**	208.1369	SE4	Kristianstad
Hisingen Logistikpark	3.7	4	**14.8**	**6**	178.4031	SE3	Göteborg
Elvireborgs Solpark	1.6	4	**6.4**	**3**	89.20154	SE4	Södra Möinge
Karlskrona Solpark	2.4	4	**9.6**	**4**	118.9354	SE4	Karlskrona
Törneby Solpark	2.25	4	**9**	**4**	118.9354	SE4	Kalmar
HSB BRF Bosvedjan	1.3	4	**5.2**	**3**	89.20154	SE3	Sundsvall
Projekt Sol 3 GWh Region Jönköping Norr	1.25	4	**5**	**2**	59.4677	SE3	Jönköping
Solpark Skas Skövde	1.2	4	**4.8**	**2**	59.4677	SE3	Skövde
Nya Solevi	5.5	4	**22**	**9**	267.6046	SE3	Göteborg
ETC Solpark	4	4	**16**	**7**	208.1369	SE3	Katrineholm
Solcellsparken I Landskrona	2.2	4	**8.8**	**4**	118.9354	SE4	Landskrona
Apotea	1.5	4	**6**	**3**	89.20154	SE3	Morgongåva
Lindbäcks	1.1	4	**4.4**	**2**	59.4677	SE2	Piteå
Solsidan	2.7	4	**10.8**	**5**	148.6692	SE4	Tvååker
Solcellsparken I Kjula	1.1	4	**4.4**	**2**	59.4677	SE3	Eskiltuna
Väla Centrum	1.1	4	**4.4**	**2**	59.4677	SE4	Helsingborg
Mega-Sol	1.1	4	**4.4**	**2**	59.4677	SE3	Arvika

Solparken	1.1	4	**4.4**	**2**	59.4677	SE3	Västerås
Vasakronan solcellspark	4.4	4	**17.6**	**7**	208.1369	SE3	Uppsala
Bredstorp Solpark	1.2	4	**4.8**	**2**	59.4677	SE3	Bredstorp
BESS Market Size - Scenario 1							
Cbn [MWh]	**975**						
No. of 40-foot BESS containers	**397**						
Total cost [USD]	**243 850 000**						